Available online at www.sciencedirect.com

SciVerse ScienceDirect

Geochimica et Cosmochimica Acta 83 (2012) 272–291

Geochimica et Cosmochimica Acta

www.elsevier.com/locate/gca

Siderophile trace elements in metals and sulfides in enstatite achondrites record planetary differentiation in an enstatite chondritic parent body

D. van Acken [a,b,c,*], M. Humayun [d], A.D. Brandon [a], A.H. Peslier [b,e]

[a] University of Houston, Dept. of Earth and Atmospheric Sciences, 312 Science & Research 1, Houston, TX 77204, United States
[b] NASA-JSC, 2101 NASA Parkway, MS KR, Houston, TX 77058, USA
[c] University of Alberta, Department of Earth and Atmospheric Sciences, 1-26 ESB, Edmonton, Alberta, Canada T6G 2E3
[d] Dept. of Earth, Ocean and Atmospheric Science and National High Magnetic Field Laboratory, Florida State University, Tallahassee, FL 32310, USA
[e] Jacobs Technology, E.S.C.G., Mail Code JE23, 2224 Bay Area Blvd, Houston, TX 77058, USA

Received 22 June 2011; accepted in revised form 16 December 2011; available online 2 January 2012

Abstract

Siderophile element concentrations were measured by LA-ICP-MS in metals and sulfides from five aubrite meteorites. Siderophile element patterns in aubrites are either similar to those in metal from enstatite chondrites, or can be derived by crystallization from metallic liquids derived by partial melting of E chondrites. Some metal grains in Mt. Egerton, Cumberland Falls, and Aubres show moderate to severe depletion in compatible highly siderophile elements (Re, Os, Ir, Ru) which are consistent with solid metal/liquid metal differentiation of enstatite chondrite-like metal. Metals from chondrite inclusions in Cumberland Falls show more extremely fractionated patterns than those from the aubritic matrix, potentially hinting at fractionation and partial melting processes affecting not only the aubrite parent body, but the chondrite body from which the inclusions were derived as well. Models using experimental partition coefficients show that aubrite metal chemically corresponds to solid metal segregated during differentiation of primary metallic liquids of EH/EL composition that contained both substantial S- and C-contents. This result is consistent with a genetic link between enstatite chondrites and aubrites, but as to whether aubrites were derived from the same body(ies) as enstatite chondrites, or have their origin in multiple, and potentially separated bodies, cannot be answered unequivocally with chemical or isotopic data alone.

1. INTRODUCTION

Aubrites, or enstatite achondrites, are differentiated reduced meteorites, most of them fragmental or regolith breccias. They consist mainly of Fe-free orthopyroxene (on average 90%, e.g. Reid and Cohen, 1967; Watters and Prinz, 1979; Keil, 2010), with plagioclase, diopside, forsteritic olivine, Fe–Ni metal, and sulfides as minor modal components (e.g. Lonsdale, 1947; Watters and Prinz, 1979). Their formation under very reducing conditions, similar to those experienced by enstatite chondrites, is reflected by incorporation into sulfide of nominally lithophile elements (Cr, Ti, Mn, Mg, Ca) as trace elements (e.g. Watters and Prinz, 1979) or as major elements with the formation of minerals such as oldhamite (CaS), alabandite (MnS), and daubreelite ($FeCr_2S_4$), among others. Based on igneous textures present in many fragments, aubrites are widely assumed to have experienced magmatic processing in one or more parent body(ies) subsequent to core formation (e.g. Graham et al., 1977; Okada et al., 1988; Keil, 1989; Wheelock et al., 1994). A common origin with enstatite chondrites is further supported by identical

* Corresponding author at: University of Alberta, Department of Earth and Atmospheric Sciences, 1-26 ESB, Edmonton, Alberta, Canada T6G 2E3. Tel.: +1 780 492 2676; fax: +1 780 492 2030.
E-mail address: vanacken@ualberta.ca (D. van Acken).

0016-7037/$ - see front matter © 2011 Elsevier Ltd. All rights reserved.
doi:10.1016/j.gca.2011.12.025

oxygen isotope composition of both groups (Clayton et al., 1984; Clayton and Mayeda, 1996). However, an origin of aubrites from the same parent body as either high-Fe (EH) or low-Fe (EL) enstatite chondrites is disputed, based on aubrite metal/sulfide ratios, Ti concentrations in sulfide, and temperature calculations (Keil, 1969, 1989; Brett and Keil, 1986; Fogel et al., 1988). The Mt. Egerton and Shallowater meteorites are anomalous compared to the other aubrites, in that they are more metal-rich and not brecciated (e.g. Keil, 2010). The anomalous enstatite achondrite Shallowater has been assigned to a different parent body than that (or those) of the aubrites, based on its higher contents of troilite (FeS) and Fe metal, the presence of plagioclase, and the absence of diopside (Keil, 1989, 2010; Keil et al., 1989).A close genetic relation to aubrites, and possibly a part of the differentiation sequence of the aubrite parent body, is suggested for the anomalous enstatite meteorite Mt. Egerton based on mineral chemistry and oxygen isotopic composition (Watters and Prinz, 1980; Casanova et al., 1993; Keil, 2010).

Because of their affinity for metal (and, for some elements, sulfide), siderophile elements may reveal a complementary perspective to constrain the accretionary and early differentiation history of the aubrite parent body (APB) than that obtained by lithophile elements. Siderophile elements partition into the metal over coexisting silicate, and thus get enriched in planetary cores. Experimentally determined partition coefficients $D^{\text{metal/silicate}}$ for siderophile elements range from ~10 up to $>10^{16}$, and are dependent on temperature, pressure, oxygen fugacity, and both silicate and metal composition (Borisov et al., 1994; Li and Agee, 1996, 2001; Borisov and Palme, 1997; Jana and Walker, 1997a,b,c; Capobianco et al., 1999; Holzheid et al., 2000; Righter and Drake, 2000; Righter, 2003; Righter et al., 2008, 2010; Mann et al., 2009; Brenan and McDonough, 2009). A subset of these elements with the highest $D^{\text{metal/silicate}}$ ($>10^6$) are termed the highly siderophile elements (HSE: Ru, Rh, Pd, Re, Os, Ir, Pt, Au). Furthermore, siderophile elements exhibit a wide range of compatibility during partial melting and can be used to study melting and differentiation processes in parent bodies. Also, the large range of condensation temperatures of siderophile elements (e.g. W, Re, Os: ~1800 K, Sn ~ 700 K, Lodders, 2003) allows study of the accretion conditions and comparison between undifferentiated materials such as enstatite chondrites and their possible differentiates such as aubrites.

Studies of metal composition in a number of stony meteorites have revealed complex histories and heterogeneous formation conditions (e.g. Wasson and Wai, 1970; Casanova et al., 1993; Kong et al., 1997; Campbell et al., 2001, 2002; Campbell and Humayun, 2003). Earlier work on aubrites provided basic characterization of the metal and sulfide phases for both major and trace elements (Keil and Fredriksson, 1963; Wasson and Wai, 1970; Watters and Prinz, 1979; Wolf et al., 1983; Easton, 1986; Casanova et al., 1993). A number of studies focused on rare earth element (REE) concentrations in oldhamite, which is a major host for REE under reducing conditions (Floss et al., 1990; Floss and Crozaz, 1993; Wheelock et al., 1994; Crozaz and Lundberg, 1995; Lodders, 1996; Dickinson and McCoy, 1997; Hsu and Crozaz, 1998). Oldhamites have REE signatures consistent with partial melting and melt extraction in the APB as well as undifferentiated signatures interpreted as remnants from nebular condensation (Floss et al., 1990; Floss and Crozaz, 1993; Lodders et al., 1993; Wheelock et al., 1994; Hsu and Crozaz, 1998). An igneous origin is further supported by Eu anomalies in plagioclase and 'magnetic' mineral fractions (Graham and Henderson, 1985; Floss and Crozaz, 1993; Dickinson and McCoy, 1997).

Heterogeneities in aubrite metals were interpreted as representing multiple compositional populations of metal (Graham, 1978; Wolf et al., 1983; Easton, 1986; Ntaflos et al., 1988). Similarities between anomalous iron meteorites and the metal fraction of some aubrites have been previously noted (Wasson, 1990). Graham (1978) and Easton (1986) considered it unlikely that aubrite metal can be derived from enstatite chondrite parentage by igneous processing on the parent body. In contrast, a link between aubrites and enstatite chondrites on the basis of aubrite metal trace element composition was inferred by Casanova et al. (1993), who proposed that aubrites could represent partial melts from enstatite chondrite parentage.

To potentially reconcile the conflicting aspects of metal and sulfide formation in aubrites and further resolve the complex history of the APB, a siderophile element study of metals and sulfides in 10 samples was performed in this study. This includes electron microprobe analysis for the major elements in aubrite sulfides and metals coupled with LA-ICP-MS analyses for siderophile trace elements.

2. SAMPLES AND ANALYTICAL METHODS

As of November 2011, the Meteoritical Society listed the total number of known aubrites as 67 (http://www.lpi.usra.edu/meteor/), but a significant number of the Antarctic aubrites are either considered paired with Allan Hills 84007 or are too small in sample size to be available for analysis via LA-ICP-MS. Further, only a subset of available sections from representative aubrites contained metal suitable for analysis, limiting our sample selection and reported data to the samples described below. Thin sections of aubrites were obtained from the Smithsonian Institution – Khor Temiki USNM 1551-2, Aubres USNM 7047-1, Mayo Belwa USNM 5873-4, Cumberland Falls USNM 477-1, Norton County USNM 1712-2, and Bishopville USNM 222-1. Thin sections for the anomalous enstatite meteorites Mt. Egerton (USNM 3272-1) and Shallowater (USNM 1206-2) were also obtained from the Smithsonian Institution. Two 150 μm thick sections were prepared by the Meteorite Working Group at NASA-Lyndon B. Johnson Space Center (JSC) from samples Allan Hills 84007,116 and LaPaz Icefield 03719,22.

Electron Microprobe analyses were conducted at NASA-JSC in Houston, on a Cameca SX100 electron microprobe. The acceleration voltage used was 15 kV, the probe current 20 nA, and the beam size 1 μm. Several spots were analyzed per grain to verify grain homogeneity. X-ray wavelength dispersive crystals used were PET for Ca, P, K, S, and Ti; LIF for Fe, Mn, and Cr; LLIF for Ni, Co, and

Cu; and TAP for Mg, Na, and Si. Calibration standards were diopside (Ca, Mg, Si), apatite (P), orthoclase (K), chromite (Cr), rhodonite or tephroite (Mn), troilite (Fe, S), rutile (Ti), pentlandite (Ni), cuprite (Cu), cobaltite (Co), and oligoclase (Na). For some metal runs, Ni and Fe were calibrated against Ni and Fe metals, respectively. Peak counting times were set to 20 s, background counting times were 10 s. In situ LA-ICP-MS analyses were conducted at the National High Magnetic Field Laboratory at Florida State University using a New Wave UP193FX excimer laser ablation system (193 nm) attached to a Thermo Element XR™ ICP-MS using procedures similar to those described previously (Humayun et al., 2007, 2010). Depending on grain size, samples were either analyzed with a 50 μm line scan at 10 μm/s scan speed, or as single spots with the beam diameter (depending on grain size) of 50–100 μm with 2 s dwell time (the duration of laser firing). Small grains in Mayo Belwa, Aubres, Bishopville, Khor Temiki, and Norton County were analyzed by spot analysis, while larger metal or sulfide grains in Mt. Egerton, Shallowater, and Cumberland Falls permitted line scans. Both modes of measurement were conducted with 20 Hz repetition rate at 100% power output (2.4 GW/cm^2, 11 J/cm^2). The peaks ^{23}Na, ^{25}Mg, ^{27}Al, ^{29}Si, ^{31}P, ^{34}S, ^{39}K, ^{44}Ca, ^{45}Sc, ^{47}Ti, ^{51}V, ^{53}Cr, ^{55}Mn, ^{57}Fe, ^{59}Co, ^{60}Ni, ^{63}Cu, ^{66}Zn, ^{69}Ga, ^{74}Ge, ^{75}As, ^{77}Se, ^{88}Sr, ^{89}Y, ^{90}Zr, ^{93}Nb, ^{97}Mo, ^{102}Ru, ^{103}Rh, ^{106}Pd, ^{120}Sn, ^{121}Sb, ^{125}Te, ^{184}W, ^{185}Re, ^{192}Os, ^{193}Ir, ^{195}Pt, and ^{197}Au were acquired in low resolution by peak jumping. The correction for $NiAr^+$ on ^{102}Ru was <5% based on analysis of Ni foil. For some analyses of metals, a reduced number of elements were used, excluding the lithophile trace elements. For standardization the relative sensitivity factors (RSFs) were determined on North Chile (Filomena) IIAB and Hoba IVB iron meteorites, NIST SRM 1263a steel (Campbell et al., 2002), MPI-DING basaltic glasses (Jochum et al., 2006; Humayun et al., 2007; Gaboardi and Humayun, 2009), and pyrite single crystals. The determination of the relative sensitivity factor for S revealed that cleaved pyrite surfaces had undergone substantial oxidation and provided too low a value of the S/Fe ratio, but a freshly polished surface provided a consistent sulfur RSF, which yielded stoichiometric S contents for troilites.

All standards were run at the beginning of each day for laser ablation ICP-MS measurements. Prior to sample measurements after sample changes, a set of three gas blanks was run. Gas blanks were insignificant for most minor and trace elements, with the exception of Ti, As, Ga, Ru, and Sn in samples low in these elements. Standard and sample count rates were corrected to the corresponding set of blanks run immediately before. Sample concentrations were calculated with relative sensitivity factors normalized to Fe concentration. Detection limits were established as 3 standard deviations for all blanks run on a particular day. Element concentrations below detection limit are reported as a maximal value corresponding to the detection limit.

3. RESULTS

3.1. Electron microprobe

Both metal and sulfide grains appear homogeneous in BSE images (Fig 1), without visual evidence for exsolution of different phases or formation as different populations. While metal grains occur isolated, all species of sulfide are found in clusters, intergrown with metal and each other. Major element composition of sulfides and metals analyzed by electron microprobe are listed in Table 1. Metal compositions are homogeneous within one section, with a few notable exceptions. While metal in Mt. Egerton, LAP 03719 and Khor Temiki is homogeneous, a clear bimodal distribution between Fe metal with about 5% Ni and

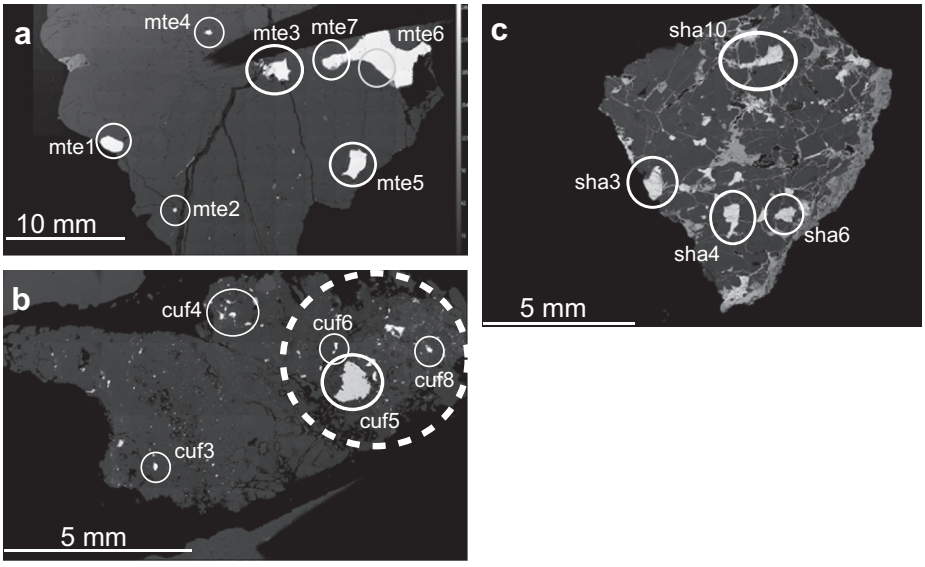

Fig. 1. Backscatter electron maps of thin sections (a) Mt. Egerton USNM 3272-1; (b) Cumberland Falls USNM 477-1; and (c) Shallowater USNM 1206-2. Sample locations for LA-ICP-MS analyses are indicated by solid circles. Dashed circle in (b): chondritic inclusion in Cumberland Falls 477-1 (Neal and Lipschutz, 1981).

Table 1
Electron microprobe analyses of enstatite achondrite metals and sulfides.

Meteorite	Section #	Phase	#	Analyses	Si	P	S	Fe	Co	Ni	Na	Mg	K	Ca	Ti	Cr	Mn	Cu	Total
Mt. Egerton	USNM 3272-1	Fe metal		234	1.85	<0.05	<0.04	90.7	0.18	5.25									98.06
			sd		0.31			3.7	0.07	3.29									
Bishopville	USNM 222-1	Troilite		130	0.03		37.1	58.2	<0.09	<0.09	<0.04[a]	<0.03	<0.03	<0.03	2.81	0.27[b]	<0.08	<0.11	98.78
			sd		0.05		0.9	2.6							1.23	0.22			
Shallowater	USNM 1206-2	Troilite		39	0.01		37.2	57.3	<0.09	0.18	<0.04	0.07	<0.03	<0.03	0.66	3.65	0.38	0.15	99.60
			sd		0.01		0.8	0.8		0.13		0.36			0.04	0.15	0.11	0.09	
Khor Temiki	USNM 1551-2	Fe metal		6	0.46		<0.04	98.5	<0.09	<0.09	<0.04	<0.03	<0.03	<0.03	<0.05	<0.06	<0.08	<0.11	99.07
			sd		0.08			1.4											
		Troilite		17	0.02		36.9	57.6	<0.09	<0.09	<0.04	<0.03	<0.03	<0.03[a]	0.45[c]	0.29[d]	<0.08[a]	<0.11	98.52
			sd		0.03		2.4	7.5							0.06	0.15			
		Alabandite		10	0.04		36.9	15.3	<0.09	<0.09	0.06	1.21	<0.03	0.21	<0.05	0.16	45.7	<0.11	99.63
			sd		0.14		0.7	1.9			0.01	0.43		0.07		0.07	3.2		
		Oldhamite		5	0.02		41.8	0.16	<0.09	<0.09	<0.04	0.27	<0.03	50.8	<0.05	<0.06	1.30	<0.11	94.34
			sd		0.05		1.5	0.09				0.12		1.5			0.56		
		Daubreelite		1	0.03		42.0	18.0	<0.09	<0.09	0.05	<0.03	<0.03	<0.03	<0.05	35.83	1.29	<0.11	97.29
			sd																
Aubres	USNM 7047-1	Fe metal		4	0.56[e]		<0.04	94.76[e]	<0.09	2.91[e]	<0.04	<0.03	<0.03	<0.03	<0.05	<0.06	<0.08	<0.11	98.93
			sd		0.33			0.6		0.56									
		Troilite		48	0.02		36.7	60.1	<0.09	<0.09	<0.04	<0.03	<0.03	<0.03	1.80	0.45	<0.08	<0.11	99.24
			sd		0.01		0.6	1.1							1.02	0.18			
		Alabandite		13	0.01		38.4	12.6	<0.09	<0.09	0.08	4.95	<0.03	0.14	<0.05	0.17	42.9	<0.11	99.23
			sd		0.01		1.2	2.6			0.05	0.79		0.05		0.37	1.7		
		Daubreelite		9	0.02		43.1	17.3	<0.09	<0.09	<0.04[a]	<0.03[a]	<0.03	<0.03[a]	0.13	35.8	1.28	0.21[f]	98.33
			sd		0.02		2.7	1.1							0.09	2.4	0.35	0.10	
Mayo Belwa	USNM 5873-4	Fe metal		8	0.88		<0.04[a]	90.8	0.15	5.27	<0.04	0.61	<0.03	<0.03	<0.05	<0.06[a]	<0.08	<0.11	97.93
			sd		3.19			6.8	0.16	3.04		3.44							
		Troilite		14	0.11		36.6	58.8	<0.09	<0.09	<0.04	<0.03	<0.03	<0.03	2.18	0.30	0.23[g]	<0.11	98.36
			sd		0.67		1.4	2.0							2.13	0.26	0.47		
		Alabandite		20	0.03		37.7	22.3	<0.09	<0.09	0.22	3.38	<0.03	0.46	0.13	0.56	33.8	<0.11	98.69
			sd		0.06		1.0	4.0			0.08	1.38		0.11	0.11	0.32	4.3		
		Oldhamite		7	0.00		41.7	0.17	<0.09	<0.09	0.05	0.34	<0.03	51.6	<0.05	<0.06	0.82	<0.11	94.68
			sd		0.01		0.7	0.18			0.03	0.15		0.8			0.33		
Norton County	USNM 1712-2	FeNi metal		5	0.18[h]		<0.04[a]	91.6[h]	0.16[g]	6.49[h]	<0.04	<0.03	<0.03	<0.03	<0.05	<0.06	<0.08	<0.11	98.66
			sd		0.11			2.0	0.15	1.85									
		Troilite		31	0.02		36.6	59.8	<0.09	<0.09	<0.04	<0.03	<0.03	<0.03	1.83	0.28[i]	<0.08	<0.11	98.93
			sd		0.07		0.6	3.2							1.38	0.12			
		Daubreelite		4	0.01		43.1	17.4	<0.09	<0.09	<0.04	<0.03	<0.03	<0.03	0.26[g]	35.5	1.29	0.39[g]	98.00
			sd		0.04		2.4	0.7							0.29	2.0	0.57	0.45	

(*continued on next page*)

Table 1 (*continued*)

Meteorite	Section #	Phase	#	Analyses	Si	P	S	Fe	Co	Ni	Na	Mg	K	Ca	Ti	Cr	Mn	Cu	Total
Cumberland Falls	USNM 477-1	Fe metal		33	<0.02[a]		<0.04	91.52	0.24	5.87	<0.04	0.07	<0.03	<0.03	<0.05	<0.06	<0.08	<0.11	97.74
			sd					2.52	0.14	0.87		0.05							
		FeNi metal		3	<0.02		<0.04[a]	61.9	<0.09	36.8	<0.04	<0.03	<0.03	<0.03	<0.05	<0.06	<0.08	<0.11	98.92
			sd					13.1		11.3									
		Troilite		23	0.06		35.9	61.5	<0.09	<0.09	<0.04	<0.03[a]	<0.03	<0.03	<0.05	0.19[e]	<0.08	<0.11	97.84
			sd		0.31		2.1	2.7								0.10			
		Daubreelite		1	0.02		43.6	18.2	<0.09	<0.09	<0.04	<0.03	<0.03	<0.03	<0.05	35.4	0.47	0.67	98.36
			sd																
ALH 84007	,116	FeNi metal		2	<0.02	<0.05	0.12	50.3	<0.09	46.00	<0.04	<0.03	<0.03	<0.03	<0.05	0.29	<0.08	<0.11	96.76
			sd																
		Fe metal		3	<0.02	<0.05	<0.04	95.3	0.42	5.77	<0.04	<0.03	<0.03	<0.03	<0.05	<0.06	<0.08	<0.11	101.64
			sd																
		Troilite		35	<0.02	<0.05	36.1	62.8	<0.09	<0.09	<0.04	<0.03	<0.03	<0.03	<0.05	0.42[b]	<0.08[a]	<0.11	99.66
			sd				2.6	2.4								0.16			
		Daubreelite		8	<0.02	<0.05	43.9	19.0	<0.09	<0.09	<0.04	<0.03	<0.03	<0.03	<0.05	36.4	0.86	<0.11	100.12
			sd				0.8	2.2								1.8	0.35		
LAP 03719	,22	Fe metal		12	0.31	<0.05	<0.04	98.6	<0.09	2.12	<0.04	<0.03	<0.03	<0.03	<0.05	<0.06[a]	<0.08	<0.11	101.23
			sd		0.13			3.2		2.63									
		Schreibersite		4	0.04	13.6	<0.04	71.7	0.11	13.4	<0.04	<0.03	<0.03	<0.03	<0.05	<0.06	<0.08	<0.11	98.92
			sd		0.04	0.4		1.3	0.03	0.4									
		Troilite		34	<0.02[a]	<0.05	35.9	59.9	<0.09	<0.09	<0.04	<0.03	<0.03	<0.03[a]	2.29	0.35[j]	<0.08[a]	<0.11	98.79
			sd				3.7	3.5							1.07	0.25			
		Alabandite		4	<0.02	<0.05	38.0	13.1	<0.09	<0.09	0.05	3.80	<0.03	0.15	<0.05	0.11	44.1	<0.11	99.29
			sd				0.3	2.4			0.02	0.19		0.02		0.05	1.9		
		Daubreelite		13	0.09[k]	<0.05	42.2	17.4	<0.09	<0.09	<0.04[a]	0.08[g]	<0.03	<0.03	0.14	35.6	1.40	0.30	97.32
			sd		0.07		2.7	0.8				0.15			0.07	1.9	0.24	0.17	

All abundances in wt.%.

sd: 2 standard deviations.

[a] Single grains above detection limit, see Supplemental Table 1.

[b] Three anomalous Cr-rich grains excluded.

[c] Anomalous Ti-rich and Ti-poor samples excluded.

[d] Two anomalous Cr-rich grains excluded.

[e] One anomalous Ni-Si-rich metal grain excluded.

[f] Two anomalous Cu-rich grains excluded.

[g] Mn in troilite in Mayo Belwa, Ti and Cu in daubreelite in Norton County, and Mg in daubreelite in LAP 03719 show extreme heterogeneity above detection limit.

[h] Two anomalous Ni-rich grains excluded.

[i] Four anomalous Cr-rich grains excluded.

[j] One anomalous Cr-rich grain excluded.

[k] One anomalous Si-rich grain excluded.

Fe–Ni metal with about 45% Ni can be seen in ALH 84007. Metal in Aubres, Norton County, Cumberland Falls, and Mayo Belwa is homogeneous within one sample section, with single (1–3) analyses per section, see Supplemental Table 1 grains showing more Ni- and Si-rich compositions compared to the predominant metal. No metal was observed in the Shallowater section (USNM 1206-2), in contrast to past studies, which reported up to 10% of modal metal content from other sections and pieces of Shallowater (Foshag, 1940; Wasson and Wai, 1970; Keil et al., 1989). Aubres contains one grain with 13% Ni intergrown with Fe metal with 3% Ni Norton County contains two Ni-rich grains, one with 21% Ni (taenite), the other with 46% Ni (tetrataenite), compared to 5–8% Ni in the other grains. The vast majority (33 out of 36) of Cumberland Falls metal grains have around 5–6% Ni, but three grains are intergrown with grains containing around 35% Ni. Schreibersite (Fe_3P) was only detected in LAP 03719, however, LA-ICP-MS analyses showed the presence of P-rich regions in large metal grains in Mt. Egerton (see below). Graham (1978) described very heterogeneous metal and schreibersite in Mayo Belwa, reporting Fe metal with Ni concentrations between 0.75% and 23.5% and several schreibersite grains with Ni between 8.12% and 14.37% and P concentrations between 15.2 and 15.8%. Easton (1986) reported Ni contents of 2.3–7.0% in metal from aubrites, along with up to 0.85% of Si. Silicon concentrations in aubrite metal for Norton County previously reported (Wasson and Wai, 1970; Watters and Prinz, 1979; Easton, 1986) are higher than those determined in our study (0.58–0.91% vs. 0.18 ± 11%). Casanova et al. (1993) have reported large variations in Si and Ni content in kamacite from ALHA 78113, Bishopville, Mayo Belwa, and Norton County, between below detection limit and 1.37 wt.% for Si, and 0.53 and 11.09 wt.% for Ni. Metal with Ni concentrations as high as 50% (tetrataenite exsolution), as seen in single Norton County and ALH 84007 grains, has previously been described for Khor Temiki (Hey and Easton, 1967).

As with metals, sulfides of a given compositional type are homogeneous throughout one section for most of their minor elements. By far the most abundant sulfide is troilite. The largest variation of minor elements in troilite, both within one section and compared to other samples, is displayed by Cr and Ti. Titanium concentration in troilite varies strongly both between sections and within one section, with Khor Temiki troilite containing as much 8.5% Ti, compared to 0.6% in Shallowater troilite and 3% in Bishopville and LAP 03719 troilite. Norton County troilite ranges from 0.75% to 3.4% Ti, in accordance with the reported values of 0.4–4.1%, with a mean of 1.7% (Keil and Fredriksson, 1963). Troilite in ALH 84007 is essentially Ti-free (0.05%). Chromium contents of troilite are around 0.1–1.0% in ALH 84007, LAP 03719, Cumberland Falls, Mayo Belwa, and Aubres. Some grains in Khor Temiki, Bishopville, and Norton County have as much as 2.8% Cr, while Shallowater troilite contains 3.6% Cr. Other than minor Cu and Ni content in Shallowater troilite, other minor elements in troilite were below detection limit of the electron microprobe. Single spots from Khor Temiki, Mayo Belwa and LAP 03719 show increased Mn of up to 1.1%. All other minor elements are below 0.2%. Keil et al. (1989) reported troilite analyses from Shallowater with 0.64% Ti and 3.35% Cr, in excellent agreement with our data.

Oldhamite has been described in a number of enstatite achondrites, but only a few grains were found during this study, intergrown with other sulfides and metal in Khor Temiki and Mayo Belwa. Other than minor amounts of Mg (0.2–0.3%) and Mn (0.8–1.3%), all other minor elements determined by microprobe are below 0.2% in oldhamites. All oldhamite analyses yield low totals between 92 and 96 wt.%, suggesting either the presence of a minor element unaccounted for or the presence of small amounts of CO_2 or H_2O from terrestrial alteration.

Alabandite is an abundant phase in Khor Temiki, Aubres, Mayo Belwa and LAP 03719. Minor element concentrations are comparable throughout these four sections, with only 3–5% Mg present and all other elements below 0.5%. In Mayo Belwa, alabandite is significantly more Fe-rich than in the other samples, with a concentration of 22% Fe. Daubreelite is present in Khor Temiki, Aubres, Norton County, Cumberland Falls, ALH 84007, and LAP 03719, occurring intergrown with troilite, alabandite, and metal. Other than Mn, which has a concentration of ~1.3% in daubreelite, no minor elements were detected.

A variety of other exotic sulfides such as niningerite (Mg, Fe, Mn)S and caswellsilverite ($NaCrS_2$) have been described in aubrites (e.g. Okada and Keil, 1982; Keil et al., 1989), none of which were found in this study. A number (3%) of microprobe analyses yielded low totals of less than 95%, suggesting the presence of H_2O or CO_2 in the analyzed grains, as described for terrestrial weathering products like schoellhornite ($Na_{0.3}(H_2O)_1[CrS_2]$) in Norton County (Okada et al., 1985). We acknowledge the likely presence of a minor amount of these phases in the aubrite sections studied, but will leave them out of the discussion, as they represent terrestrial alteration and weathering products and do not contribute to our understanding of the formation and differentiation of metal and sulfides on the APB.

3.2. LA-ICP-MS results for minerals

Results from in situ measurements of Fe–Ni metals and troilite by LA-ICP-MS are listed in Table 2. Samples from Mt. Egerton, Shallowater and Cumberland Falls represent analyses of large metal or troilite grains taken by line scans, while analyses from Aubres and Mayo Belwa are spot analyses. Backscattered electron image maps with the sample locations within the respective sections for Mt. Egerton, Cumberland Falls, and Shallowater are shown in Fig 1. Analyses from metal and sulfide in Bishopville, Norton County, and Khor Temiki did not yield siderophile element concentrations above background level, mostly due to the small grain sizes of less than 30 μm for metals and low siderophile element concentrations in larger sulfide grains, and are excluded from the discussion.

Based on the siderophile element characteristics, the presentation of LA-ICP-MS results are subdivided into (a) Mt. Egerton, (b) aubrites *sensu stricto*, including Cumberland Falls, Aubres, and Mayo Belwa, and (c) Shallowater. The

Table 2
Elemental abundances bu LA-ICP-MS (ppm, except where noted).

	Shallowater				Mt. Egerton										Cumberland Falls							Aubres		Mayo Belwa				
	USNM 1206-2				USNM 3272-1										USNM 477-1							USNM 7047-1		USNM 5873-4				
	sha3	sha4	sha6	sha10	mte1	mte2	mte3	mte3	mte4	mte5	mte6	mte6	mte7	mte7	mte8	cuf3	cuf4	cuf4	cuf5	cuf5	cuf6	cuf8	aub7	aub7	may2	CI normalizing values			
								P-rich						P-rich												A&G 1989	H 2003	F-G 2010	Average
	Troilite	Troilite	Troilite	Troilite	Metal	Metal	Metal	Metal	Metal	Metal	Metal	Metal	Metal	Metal	Metal	Metal	Metal	Metal	Troilite	Troilite	Metal	Metal	Metal	Metal	Metal				
Na	<928	<687	<842	<448								<1755			2656											5000			5000
Mg	3901	1122	1052	969								<12			539											989000			989000
Al	59	134	287	410								<85			225											8680			8680
Si (wt.%)	0.5	0.3	0.4	0.6	3.3	2.6	4.8	11.4	2.9	2.9	2.3	1.3	3.3	16.3	4.6	5.1	4.8	4.6	7.1	6.0	3.7	16.9	1.5	2.0	2.3	10.64			10.64
P	<44	246	<40	419	1228.8	554	1156	138628	282	961	670	530	1300	68602	298	684	955	962	<124	<522	1391	572	673	967	2737	1220			1220
S (wt.%)	34.8	32.7	35.3	32.6	<0.5	<0.4	<0.1	0.3	<0.1	<0.1	<0.04	<1.9	<0.1	1.3	5.2	<0.9	<0.9	<0.9	35.2	38.8	<0.5	<0.9	<0.3	<0.4	<0.4	6.25			6.25
K	<143	<106	<130	<90								<271			10463											558			558
Ca	<2356	<1745	<2138	1760								<4457			<1501											9280			9280
Sc	1.6	1.8	1.5	2.1								<1.6			118											5.82			5.82
Ti	5268	5272	5139	4976								<15			893											436			436
V	771	781	765	746	<2.4	<7.1	4.9	11	<11	<0.3	<0.2	<0.6	4.0	0.9	226	<4.1	<3.9	<3.6	198	30	2.8	67	<1.2	<1.6	<1.9	56.5			56.5
Cr	28500	27900	28400	31300	24.5	25	29	285	3.8	4.9	13	<853	20	137	72200	<25	70	<22	17700	10700	129	3161	31	13	<11	2660			2660
Mn	3655	3498	3656	3568								<72			17918											1990			1990
Fe (wt.%)	59.9	62.4	60.2	61.3	90.8	92.0	90.0	63.4	91.9	91.6	92.2	91.9	90.7	65.8	78.8	92.9	93.6	94.2	55.8	57.4	89.7	77.9	94.1	93.7	93.4	19.0			19.0
Co	285	512	132	602	3322.1	3223	3478	1392	2954	3540	3377	3549	3536	2016	435	2708	4250	4059	4.3	<5.3	3895	4132	2063	2114	3019	502			502
Ni (wt.%)	0.4	0.6	0.2	0.9	4.8	4.9	7.3	10.8	5.0	5.0	5.6	5.2	3.5	6.5	0.7	5.6	5.4	5.1	0.03	0.03	5.7	4.1	4.7	4.6	5.7	1.10			1.10
Cu	990	984	990	1046	131.3	98.4	114.9	97.1	66	94	104.4	122	114.6	83.0	672	28	48	25	145	156	28	23	42	43	22	126			126
Zn	249	176	119	153	<4.7	2.2	5.1	107.4	1.6	0.97	0.66	<2.6	1.9	2.7	10	45.3	105.5	<4.0	9.9	10.1	3.1	9.3	2.4	<1.8	<2.0	312			312
Ga	0.3	0.23	0.4	0.10	30.7	38.5	30.4	6.3	31	32	34.1	37	34.7	15.2	11	18.7	20.5	16.1	0.45	<1.8	16.2	13	25	26	26	10.0			10.0
Ge	1.8	4.4	1.2	6.2	88.4	128.3	93.1	8.5	92	94	94.5	102	98.7	45.6	30	115	110	105	1.3	1.6	106	80	85	92	42	32.7			32.7
As	0.09	0.24	<0.1	0.8	12.8	10.5	11.3	3.4	10.4	12.3	6.0	15	11.3	6.3	4.2	13.5	11.3	9.8	11.8	7.2	16.4	16	4.4	7.5	5.6	1.86			1.86
Se	200	194	196	309								<1.8			653											18.6			18.6
Sr	<0.8	0.9	3	0.5								<1.5			6.4											7.80			7.8
Y	0.01	0.09	0.05	0.10								<0.02			1.3											1.56			1.56
Zr	7.2	7.6	6.9	6.7								<0.01			21											3.94			3.94
Nb	7.5	7.5	7.5	7.2	<0.03	0.1	0.01	0.32	<0.16	<0.004	<0.003	<0.02	<0.02	<0.004	0.2	<0.06	<0.06	<0.05	0.77	0.75	0.04	0.2	<0.02	<0.02	<0.03	0.246			0.246
Mo	2.3	2.5	2.3	2.3	3.6	3.5	3.9	32.5	2.8	4.0	4.5	3.9	4.0	20.7	2.0	3.1	3.6	4.1	1.4	1.4	4.7	4.0	1.9	1.5	3.8	0.928			0.928
Ru	<0.1	0.09	<0.1	0.10	3.0	2.2	3.4	2.8	3.9	3.5	4.0	3.6	3.6	2.9	1.0	1.8	5.5	5.3	<0.11	<0.5	1.1	0.4	0.6	0.4	3.2	0.712	0.636	0.627	0.658
Rh	0.04	0.05	0.04	0.06	0.51	0.4	0.64	0.25	0.7	0.6	0.7	0.8	0.68	0.39	0.3	<0.5	0.8	0.9	<0.15	<0.6	<0.3	<0.5	<0.15	<0.21	0.9	0.134	0.128	0.130	0.131
Pd	<0.2	<0.1	<0.2	<0.1	2.3	2.2	2.5	1.9	2.3	2.4	2.7	2.9	2.6	2.0	1.1	2.4	2.7	2.3	<0.12	<0.5	2.6	2.2	2.0	1.9	2.7	0.560	0.554	0.567	0.560
Sn	0.16	0.19	0.16	0.7	0.68	1.5	0.6	1.5	0.6	0.67	0.79	0.3	0.7	0.33	0.17	10.5	9.5	8.8	0.5	<1.1	8.6	5.9	14.5	5.8	3.4	1.72			1.72
Sb	0.01	0.02	0.03	0.04	0.5	0.6	0.4	0.3	0.4	0.4	0.2	0.4	0.4	0.19	0.13	0.6	0.5	0.5	0.4	0.4	0.7	0.52	0.15	0.4	0.21	0.142			0.142
Te	7.9	7.7	7.7	9.9								0.17			1.1											2.32			2.32
W	0.005	0.03	0.04	0.04	0.54	0.42	0.57	0.49	0.60	0.57	0.60	0.6	0.55	0.48	0.2	0.6	0.7	0.7	0.02	0.21	0.7	0.65	0.7	0.7	0.5	0.093			0.093
Re	0.02	0.11	0.005	0.15	0.20	0.10	0.21	0.04	0.23	0.20	0.22	0.24	0.20	0.09	0.01	0.11	0.3	0.3	<0.003	<0.013	0.01	<0.004	0.02	0.02	0.20	0.037	0.036	0.037	0.037
Os	0.003	0.05	0.01	0.05	2.0	0.70	2.4	0.23	2.9	2.1	2.3	2.2	2.2	1.08	0.8	0.9	3.3	3.3	<0.002	<0.01	0.04	0.06	<0.002	<0.003	1.8	0.486	0.448	0.450	0.461
Ir	0.0004	0.02	0.001	0.02	1.9	0.76	2.3	0.18	2.7	2.0	2.0	2.2	2.1	1.00	0.7	0.8	3.1	3.0	<0.001	0.03	0.04	0.05	0.003	0.003	1.0	0.481	0.430	0.418	0.443
Pt	0.02	0.11	0.01	0.13	3.8	2.3	4.6	0.33	5.2	4.1	3.5	4.3	4.6	2.12	1.1	1.9	6.7	6.4	<0.006	<0.02	0.3	0.12	0.01	<0.008	3.6	0.990	0.855	0.871	0.905
Au	0.03	0.09	0.08	0.07	1.3	1.4	1.11	0.10	1.17	1.2	0.77	1.2	1.20	0.55	0.21	1.1	1.1	0.92	<0.04	<0.17	1.0	0.84	0.64	1.0	1.0	0.140		0.149	0.145

CI normalizing values after Anders and Grevesse (1989), Horan et al. (2003), and Fischer-Gödde et al. (2010).
Three letter + number designations refer to meteorite name and location, see Fig. 1. sha: Shallowater; mte: Mt. Egerton, cuf: Cumberland Falls; aub: Aubres, may: Mayo Belwa.

siderophile element patterns are normalized to Ni-content and CI chondrite abundances. Abundances of siderophile elements in CI chondrites from Anders and Grevesse (1989) were supplemented with new highly siderophile element (HSE) data from Horan et al. (2003) and Fischer-Gödde et al. (2010), and the resulting new CI normalization values are given in Table 2.

3.2.1. Mt. Egerton

Results from measurements of Mt. Egerton metals are displayed as CI-, Ni- normalized patterns in Fig 2a). Mt. Egerton patterns are mostly flat in terms of refractory siderophile elements (W, Re, Os, Ir, Pt, Ru), with one exception (mte2) showing slight depletions in the elements most compatible in solid metal over liquid metal (Re, Os, Ir, and Ru) down to values as low as 0.3 times CI. Normalized patterns from metal in Mt. Egerton are similar to normalized patterns from metal in enstatite chondrites (Kong et al., 1997, Fig. 2b and c), with a closer similarity to EL metal than EH metal. They show little fractionation for the more refractory elements combined with an overall depletion for volatile elements from Au through Sn, with a marked negative Cu spike. In addition to metal, the host phases of Cu include troilite and schreibersite that display prominent Cu enrichments, making Cu abundances less useful in understanding processes affecting metals. Some LA-ICP-MS measurements in mte3 and mte7 revealed irregularly distributed P-rich regions, which were not encountered during electron microprobe analysis. The overall abundance patterns of these P-rich regions are similar to their metal hosts, yet they show enrichment of Ni and Mo by up to 25% for Ni and 500–800% for Mo (P-rich portion of mte3 and mte7, Table 2), confirming previously reported affinity of these elements with phosphides (Corrigan et al., 2009).

As one metal grain (mte7) in our Mt. Egerton section occurs in association with rounded sulfide grains (Fig. 3), measurements of siderophile elements in such equilibrium assemblages may hold clues about partitioning behavior between metal and sulfide during cooling under extremely

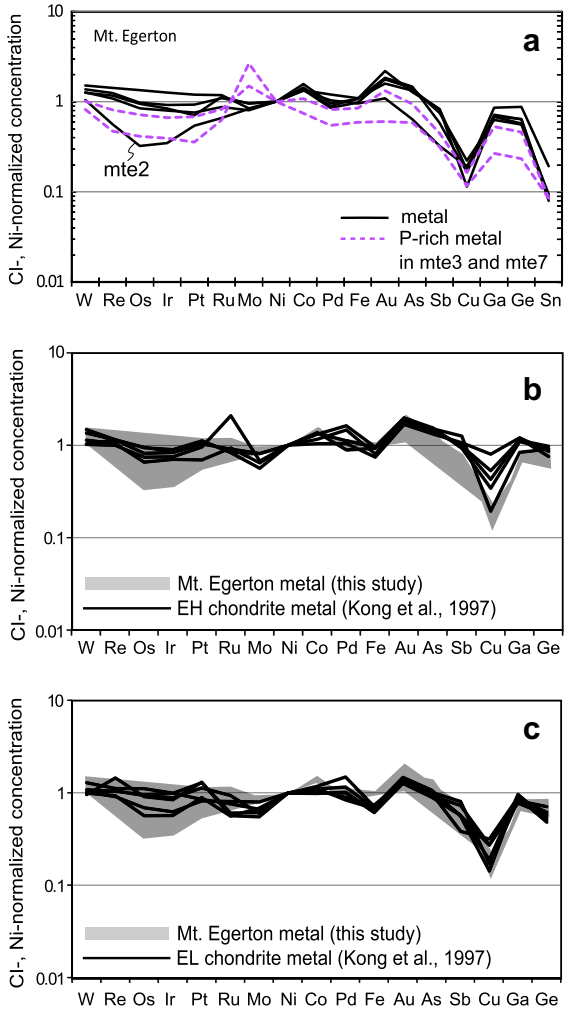

Fig. 2. CI-, Ni-normalized siderophile elements patterns for metal in the anomalous enstatite achondrite Mt. Egerton: (a) Mt. Egerton metal, dashed purple lines: P-rich regions within Mt. Egerton metal grains mte3 and mte7; (b) and (c): CI-, Ni-normalized siderophile elements patterns of Mt. Egerton metal compared to patterns from enstatite chondrite bulk metal from Kong et al. (1997). (a) EL chondrites; (b) EH chondrites, shaded area in both figures: Mt. Egerton metal analyses from this study. Concentrations for CI chondrite taken from Anders and Grevesse (1989), Horan et al. (2003), and Fischer-Gödde et al. (2010), see Table 2. (For interpretation of the references to color in this figure legend, the reader is referred to the web version of this article.)

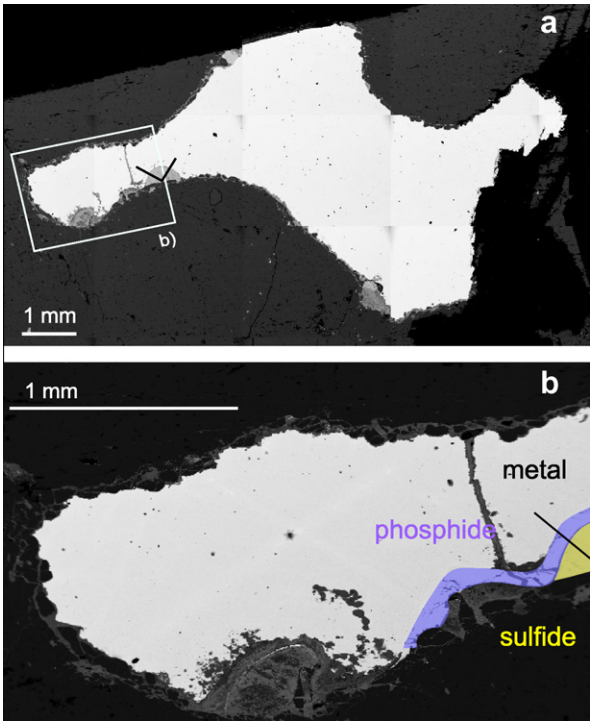

Fig. 3. (a) Backscatter electron image of Mt. Egerton grain mte7. (b) magnified area of coexisting metal, phosphide (purple) and sulfide (yellow). Black solid line: track of the laser ablation path across metal, phosphide, and sulfide. (For interpretation of the references to color in this figure legend, the reader is referred to the web version of this article.)

reducing conditions. Fig 3 shows a large metal grain with sulfide nodules at its margin. A Si-rich schreibersiterim armors the Mn–Mg-rich sulfide nodule, likely Mg-rich alabandite, from the metal. One laser traverse across the metal–phosphide–sulfide boundary was performed as marked in Fig 3. Compositions of the three phases are presented in Table 3, and the abundances of P and S are shown as a function of distance in Fig 4. While the boundaries between the metal and phosphide appear to be sharp, the boundary between phosphide and sulfide appears more gradual due to wash-out of the P signal (Fig. 4a). The underlying geometry of the grain boundaries is not evident from Fig 4, and phosphide underlying sulfide may also contribute to the gradual decline of the P signal. Segments where the analysis signals from different phases potentially overlap because of washout effects or grain geometry were excluded. The three resulting siderophile element patterns (metal, phosphide, and sulfide) are presented in Fig 4b. The metal, which comprises the largest part of this grain cluster (Fig. 4a), has abundance patterns similar to other metal grains in Mt. Egerton (Fig. 2a). The phosphide and sulfide patterns show several noticeable differences compared to metal patterns (Fig. 4b). Both phosphide and sulfide are depleted in almost all siderophile elements to a comparable degree of about one order of magnitude, with the exception of Mo, Fe, Cu, and Sn. For the refractory elements both phosphide and sulfide show very similar patterns. Concerning the more volatile elements, sulfide has higher Fe, Sb, Cu, Ge, and Sn contents than phosphide does. Both patterns somewhat mirror the overall depletion

Table 3
Trace element concentration in metal, P-rich metal, and sulfide, and apparent partition coefficients.

	Mt. Egerton			Apparent partition coefficients $D^{a/b}$		
	mte7 metal Fe metal	mte7 Phosphide Schreibersite	mte7 Sulfide Mg-rich Alabandite	Metal/phosphide	Phosphide/sulfide	Metal/sulfide
Na	<2099	1044	1427	n.d.	0.73	
Mg (wt.%)	0.05	0.21	0.83	0.24	0.25	0.06
Al	<102	<50	<24	n.d.	n.d.	
Si	<4200	<13000	<4000	n.d.	n.d.	
P (wt.%)	0.06	5.91	0.08	0.01	72.7	0.78
S (wt.%)	bdl	11.4	38.7	n.d.	0.30	
K	<324	<160	<75	n.d.	n.d.	
Ca	<5330	<2300	2834	n.d.	n.d.	
Sc	<2	36.8	127	n.d.	0.29	
Ti	<18	15.8	18.1	n.d.	0.87	
V	<0.7	2.71	13.3	n.d.	0.20	
Cr	<1020	945	3287	n.d.	0.29	
Mn (wt.%)	0.11	6.8	28.9	0.02	0.24	0.004
Fe (wt.%)	90.6	60.4	23.0	1.50	2.62	3.93
Co	3537	1380	24.2	2.56	57.1	146
Ni (wt.%)	5.12	13.5	1.43	0.38	9.49	3.59
Cu	106	147	130	0.72	1.14	0.82
Zn	<3.1	<1.5	1.57	n.d.	n.d.	
Ga	34.9	7.4	0.16	4.71	45.3	213
Ge	98	20.6	1.71	4.78	12.0	57.4
As	16.7	5.5	0.15	3.01	37.3	112
Se	<2.9	45.3	204	n.d.	0.22	
Sr	<1.8	<0.9	<0.4	n.d.	n.d.	
Y	<0.02	0.03	0.16	n.d.	0.15	
Zr	<0.01	0.04	0.25	n.d.	0.15	
Nb	<0.02	<0.02	0.02	n.d.	n.d.	
Mo	3.65	25.0	0.47	0.15	53.5	7.82
Ru	3.35	2.92	0.05	1.15	59.3	67.9
Rh	0.77	0.29	0.02	2.63	16.9	44.6
Pd	2.85	2.41	<0.26	1.18	n.d.	
Sn	0.39	0.12	0.13	3.29	0.91	3.00
Sb	0.40	0.09	0.01	4.33	7.00	30.3
Te	<0.08	0.83	0.21	n.d.	4.05	
W	0.51	0.38	0.01	1.35	35.8	48.2
Re	0.20	0.06	0.00	3.69	15.4	56.7
Os	1.98	0.47	0.01	4.23	47.3	200
Ir	1.99	0.42	0.01	4.72	54.0	254
Pt	4.19	0.90	0.02	4.68	50.4	236
Au	1.15	0.25	0.01	4.58	45.7	209

All concentrations in ppm, except where indicated.

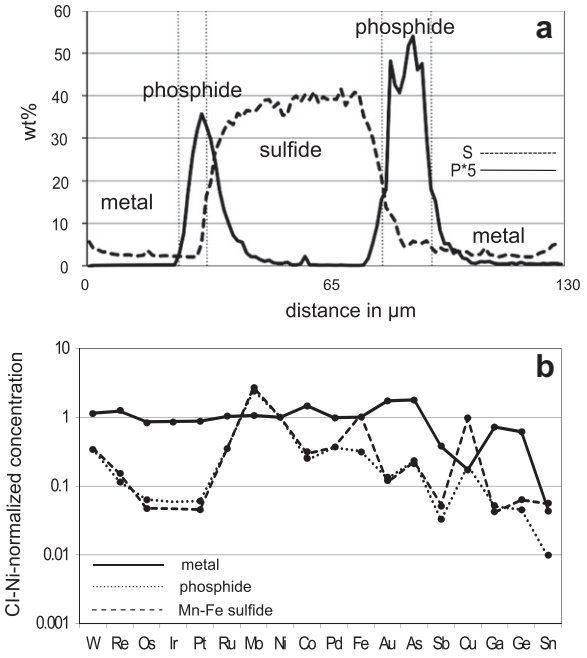

Fig. 4. (a) Concentration (wt.%) versus distance (µm) for analysis of Mt. Egerton grain mte7 for P (solid line, content multiplied by 5 for scaling purposes) and S (dashed line) b) CI-, Ni-normalized siderophile element patterns for metal (solid line), phosphide (dotted) and Mg-rich alabandite (dashed) in anomalous enstatite achondrite Mt. EgertonConcentrations for CI chondrite taken from Anders and Grevesse (1989), Horan et al. (2003), and Fischer-Gödde et al. (2010), see Table 2.

trend towards volatile elements seen in the patterns in Mt. Egerton.

3.2.2. *Aubrites sensu stricto*

Measurements in the aubrites Aubres, Bishopville, Cumberland Falls, Khor Temiki, Mayo Belwa, and Norton County were conducted on metals and several sulfides (troilite, daubreelite, alabandite, oldhamite). Analysis of metal was restricted by the grain size of metal phases encountered in the sections available, and no results could be obtained for metals in Bishopville, Khor Temiki, and Norton County. With the exception of one troilite grain in Cumberland Falls (cuf5, Table 2), sulfides of any kind did not yield siderophile trace element concentrations above their detection limits. A single metal grain from Mayo Belwa and two metal grains from Aubres were analyzed (Table 2). Five metal grains, and the one troilite were analyzed from the section of Cumberland Falls (Table 2).

Cumberland Falls section USNM 477-1 stands out, because it contains both brecciated aubrite matrix and a chondritic inclusion (Neal and Lipschutz, 1981). Metals from both within the chondritic inclusion (cuf6, cuf8) and from the aubritic matrix (cuf3, cuf4) were analyzed (Fig. 1b). Two different grains were analyzed from the area labeled cuf4 (Fig 1b). All patterns are homogeneous in terms of the more volatile siderophile elements (Pd through Sn), with a marked depletion in Cu, similar to Mt. Egerton (Figs. 2a and 5a). Of note, patterns from the aubrite matrix differ greatly from patterns from within the inclusion. Compatible HSE are enriched up to two times CI in cuf4, whereas cuf3 shows a moderate depletion to 0.3–0.5 CI

Table 4
$D^{\text{solid metal/liquid metal}}$ values used for modeling.

	Starting composition	S-rich Chabot et al., 2003, 2009		C-rich Chabot et al., 2006, 2008	
		Parameters		4% C	2% C
		D_0	β	D	D
W	0.67	1.2	3.6	0.24	0.7
Re	0.27	2	5	1.6	1.7
Os	2.88	2	5.1	7	2.5
Ir	2.69	1.5	4.9	14	2.5
Pt	7.20	0.81	4.4	9	1.7
Ru	3.40	2.6	3.4	2.4	1.5
Mo	4.10	0.9	1.1	0.3	0.25
Ni	7.52 wt.%	0.86	0.6	1.42	1.03
Co	0.37 wt.%	1.2	1.1	1.19	1.03
Pd	4.10	0.43	1.1	2.1	0.8
Fe	88.0 wt.%	[a]	[a]	[a]	[a]
Au	1.31	0.27	2.1	1.7	0.56
As	12.6	0.25	1.9	0.4	0.31
Sb	0.59	0.05	1.5	0.55	0.28
Cu	201.0	[a]	[a]	1.57	0.92
Ga	60.3	0.78	2.6	3	1.1
Ge	128.0	0.66	3	1.6	0.8
Sn	2.96	0.1	1.1	0.55	0.28

Parameters from Chabot and Jones (2003), Chabot et al. (2003, 2009).
Starting composition: EL chondrite from Kong et al. (1997), values in ppm unless noted otherwise.
Sn concentration for starting material calculated from bulk meteorite concentrations (Wasson and Kallemeyn, 1988).
[a] Cu concentration for S-rich composition scales linearly with S content (Chabot et al., 2009); Fe concentration calculated as 100% minus Ni, Co, and minor element (S or C) for each model composition.

for Re, Ir, Os, Pt, and Ru. The two patterns from within the chondritic inclusion however, have strong depletions of up to two orders of magnitude in compatible HSE such as Re, Os, and Ir (Fig. 5a). The single grain analyzed in Mayo Belwa has a similar abundance pattern to the cuf4 grains, albeit with slightly more depletion in compatible HSE Os, Ir, Pt, and Ru. The two Aubres grains show depletion of compatible HSE even more pronounced than the metal in Cumberland chondritic inclusions (cuf6 and cuf8; Fig. 5b).

3.2.3. Shallowater

In contrast to previous observations in other sections (Keil et al., 1989), Shallowater section USNM 1206-2 does not contain metal, but instead has abundant troilite (Table 1). Observed patterns in four large troilite grains are fairly homogeneous, with some minor exceptions (Fig. 5c). The Shallowater troilite has around 0.2–0.9 wt.% of Ni, compared to 4.5–10.8 wt.% in metal in Mt. Egerton, Cumberland Falls, Aubres, and Mayo Belwa, so that on the Ni-normalized abundance plot, Fe is strongly enriched by roughly an order of magnitude compared to Ni. Enrichment in Cu by a factor of 10 can be attributed to its chalcophile character, while enrichments in Mo by a similar factor are not expected from its partitioning behavior in experimental solid metal–liquid metal partitioning where Mo exhibits an increasingly compatible character with increasing sulfur content of the liquid (Chabot et al., 2006). Interestingly, Mo depletion in separated bulk metal from EH and EL chondrites is also apparent in the data of Kong et al. (1997), indicating that this is a ubiquitous effect in metal from Enstatite meteorites. Further, Mo deficiencies in metal and accompanying enrichments in troilite were also found in an in situ study of EH chondrites (Cook et al., 2004), which indicate that extremely reducing conditions (or a higher sulfur fugacity) is an influential factor on Mo distribution in enstatite meteorites. All grains show depletion in Re, Os, Ir, and Ga between one and three orders of magnitude, and, to a minor extent in Pt, Ru, Pd, Au, and As, by less than one order of magnitude. One grain (sha6) has high W/Re, and shows even slight enrichment of Pd and Au. Most striking are the high Re/Os ratios which may be relevant to obtaining internal Re–Os isochrons based on troilite (Re ~ 0.02–0.15 ppm; Os ~ 0.003–0.05 ppm) and metal (Re ~ 0.2 ppm; Os ~ 2 ppm), as previously observed for troilite–metal partitioning in IAB iron meteorites (Shen et al., 1996).

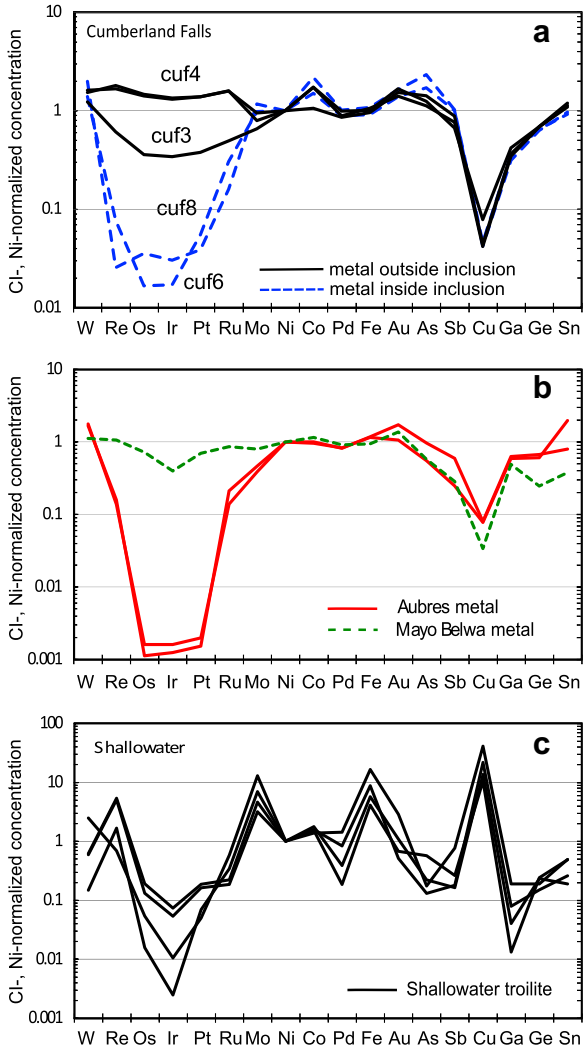

Fig. 5. CI-, Ni-normalized siderophile elements patterns for metals and sulfides in enstatite achondrites: (a) Cumberland Falls metal, black solid lines: samples outside chondritic inclusion; dashed blue lines: samples from within the chondritic inclusion; (b) solid red lines: Aubres metal, dashed green line: Mayo Belwa metal; (c) Shallowater troilite. Concentrations for CI chondrite taken from Anders and Grevesse (1989), Horan et al. (2003), and Fischer-Gödde et al. (2010), see Table 2. (For interpretation of the references to color in this figure legend, the reader is referred to the web version of this article.)

4. DISCUSSION

Metal phases of Mt Egerton and aubrites broadly have two types of siderophile elements patterns. One resembles that of chondrites (Mt. Egerton), especially enstatite EL chondrites (Kong et al., 1997), with little fractionation of the refractory elements (W to Ni, Figs. 2 and 5). The second type (including Mayo Belwa, etc.), characterized by Os, Ir and Pt depletions, testifies to post accretion phenomena such as melting and fractional crystallization (e.g. van Niekerk et al., 2009). Differences in volatile elements such as Ga, Ge, and Sn are difficult to reconcile with planetary differentiation processes. The siderophile element patterns of the sulfides and phosphides are useful to decipher metal/sulfide partitioning during metal solidification and planetary differentiation. Detailed interpretations for each meteorite as well as their siderophile element modeling are presented next.

4.1. Mt. Egerton

Most of the Mt. Egerton siderophile element patterns of metals are close to bulk metal in both EL and EH chondrites (Kong et al., 1997), with little fractionation (Fig. 2b and c). Several common features of the patterns shed light on the formation history of Mt. Egerton metal: the notable

negative anomalies in Cu and Sn, the broadly chondritic concentrations for refractory elements W – Ni and the slight depletion towards more volatile elements of As to Sn. The Mt. Egerton metals have siderophile element patterns resembling those of EL metal more closely than those of EH metal for the most volatile elements where this distinction becomes possible.

The results presented here confirm earlier findings, especially the mostly unfractionated siderophile element abundances in Mt. Egerton metal for the subset of elements analyzed by Casanova et al. (1993; Ir, Au, Ga, W, As, Re). Nickel contents in Mt. Egerton samples between 4.8 and 10.8 wt.% in this study are lower on average than those measured by Casanova et al. (1993), which have values of 9.7–9.9 wt.%. Casanova et al. (1993) ascribed these high concentrations to contamination by taenite or schreibersite, which preferentially incorporate Ni. In this study, neither taenite nor schreibersite could be detected by electron microprobe, yet variation of P content in metal of up to 13% along laser ablation tracks indicate the presence of P-rich exsolution lamellae within Mt. Egerton metal grains. This may affect the concentration of elements that preferentially partition into P-rich phases, like Ni and Mo. To investigate this possibility, we analyzed P-rich regions in two Mt. Egerton metal grains (Fig. 2) and a detailed discussion of metal–phosphide–sulfide partitioning can be found below in Section 4.1.2. Casanova et al. (1993) described siderophile element abundances of Mr. Egerton metal that are approximately chondritic for a subset of siderophile elements (Ni, Co, Cr, Ir, Au, Ga, W, As, Re), which is confirmed in this study. From their observations, they concluded that Mt. Egerton metal did not undergo fractional crystallization in a solidifying planetary core. In contrast to their observations, some Mt. Egerton patterns in this study (mte2) show a moderate degree of depletion in compatible HSE of 0.3–0.5 times CI (Os, Ir, Re; Fig. 2a). This is consistent with fractionation during solid metal/liquid metal equilibrium and removal of around 10% of a solid phase.

4.1.1. Comparison to the anomalous enstatite meteorite Northwest Africa 2526

Patterns in Mt. Egerton look broadly similar to HSE patterns from the anomalous enstatite meteorite NWA 2526 (Humayun et al., 2009), with some exceptions (Fig. 6). The reason for the Mo discrepancy may lie in the presence and irregular distribution of P-rich domains which show preferred accommodation of Mo into these domains. The pattern in Mt. Egerton metal does not share the same level of enrichment in Re–Os–Ir with NWA 2526, and also has a super-chondritic W/Re ratio, while the NWA 2526 metal has a sub-chondritic W/Re ratio (Fig. 6). These differences can be accommodated by having Mt. Egerton metal crystallize from a liquid that left NWA 2526 as a residue. This is supported by the different amounts of depletion in compatible HSE in different metal grains from Mt. Egerton (Fig. 6), which could be interpreted as progressive differentiation during crystallization. NWA 2526 was described as a coarse-grained enstatite meteorite with ~85% enstatite and 10–15% of kamacite and weathering products

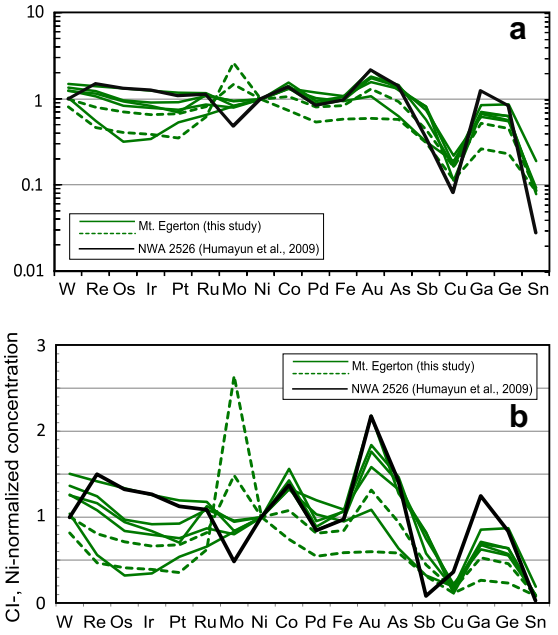

Fig. 6. CI-, Ni-normalized siderophile element patterns for metal from anomalous enstatite meteorite NWA 2526 (Humayun et al., 2009). Solid green lines: Mt. Egerton metal; dashed green lines: P-rich Mt. Egerton metal samples from this study (see Fig. 2a). Concentrations for CI chondrite taken from Anders and Grevesse (1989), Horan et al. (2003), and Fischer-Gödde et al. (2010), see Table 2. (For interpretation of the references to color in this figure legend, the reader is referred to the web version of this article.)

(Keil and Bischoff, 2008). Based on petrography, it was interpreted as a partial melt residue after ~20% melt extraction from an enstatite chondrite-like parent lithology (Keil and Bischoff, 2008), followed by slow subsolidus cooling. Siderophile element signatures of NWA 2526 have been interpreted to result from removal of up to 40–60% of both S- and C-bearing metallic liquids (Humayun et al., 2009).

The complementary HSE patterns in metal from these two anomalous metal-rich enstatite meteorites could suggest a common origin. Keil and Bischoff (2008) placed NWA 2526 on an enstatite chondrite-like planetary body distinct from the EL, EH, aubrite and Shallowater bodies based on high metal content, low abundance of troilite, absence of plagioclase and recrystallized texture of the meteorite. Thus, the anomalous enstatite meteorites Mt. Egerton and NWA 2526 as well as Itqiy (Keil and Bischoff, 2008) may originate from the same planetary body.

4.1.2. Partitioning between P-poor metal, phosphide and sulfide

The sulfide grains, separated from metal by a P-rich metal rim, may have formed in equilibrium with metal, potentially as high temperature segregates, based on their rounded grain boundaries towards metal/phosphide and sharp contact with surrounding silicate (Fig. 3). From the concentrations of siderophile elements in metal, P-rich metal and Mn–Fe sulfide, rough estimates of partition coefficients between these phases stable under reducing conditions can be obtained. Apparent partition coefficients $D^{\text{metal/P-rich metal}}$ and $D^{\text{P-rich metal/sulfide}}$ are listed in Table 3.

Siderophile elements (Co, Ga, Ge, As, Ru, Rh, Pd, W, Re, Os, Ir, Pt, Au) have apparent partition coefficients between 1.0 and 2.9 between metal and phosphide, and between 9.2 and 25.0 between phosphide and sulfide (Table 3). Calculated $D_{metal/sulfide}$ coefficients for these range from ~10 to ~70 (Table 3). Based on the paucity of experimental partitioning studies in P-bearing metal systems which are generally limited to a temperature range above the solidus, it is difficult to validate these apparent partition coefficients against experimentally determined values. The majority of previous studies report data only for a limited number of elements, mostly Au, Ga, Ge, and Ir (Willis and Goldstein, 1982; Malvin et al., 1986; Jones and Malvin, 1990), whereas a fuller set of partition coefficients was determined by Corrigan et al. (2009). Additionally, these studies focussed on liquid metal/solid metal partitioning in P-bearing metal-alloy systems. Given the similar depletion in Os, Ir, Co, Pd, As, Sb, and Sn of the Si-rich phosphide and Mn–Fe sulfide patterns in Mt. Egerton (Fig. 4b), the phosphide is interpreted to have formed under the strong influence from the sulfide, not from the metal. However, the strong affinities of Ni, Mo, and, to a minor extent, Ru for the P-rich phase are consistent with previous findings (Campbell et al., 2003; Corrigan et al., 2009), as are the weak tendencies of phosphide avoidance for Ga, Ge, Ir, and Au (Corrigan et al., 2009). Interestingly, both As and Sb are members of Group V of the periodic table, which includes P, but are depleted relative to P partitioning between phosphide and metal.

4.2. Aubrites

Siderophile element patterns in metal from aubrites *sensu stricto* (Cumberland Falls, Aubres, Mayo Belwa) share some of the characteristics with patterns in Mt. Egerton (Figs. 2a and 5a and b). All aubrite patterns have a similar negative Cu anomaly, like Mt. Egerton metals, indicative of removal of Cu by a sulfide phase and consistent with deri-

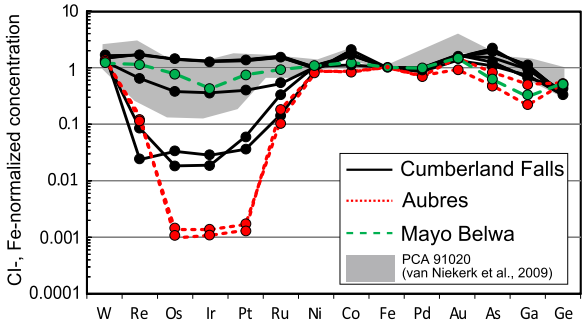

Fig. 7. CI-, Ni-normalized siderophile element patterns of metals in Cumberland Falls (black solid lines), Aubres (red dotted lines) and Mayo Belwa (green dashed line) compared to patterns from metal in EL3 chondrite PCA 91020 (gray shaded area, van Niekerk et al., 2009). Concentrations for CI chondrite taken from Anders and Grevesse (1989), Horan et al. (2003), and Fischer-Gödde et al. (2010), see Table 2. (For interpretation of the references to color in this figure legend, the reader is referred to the web version of this article.)

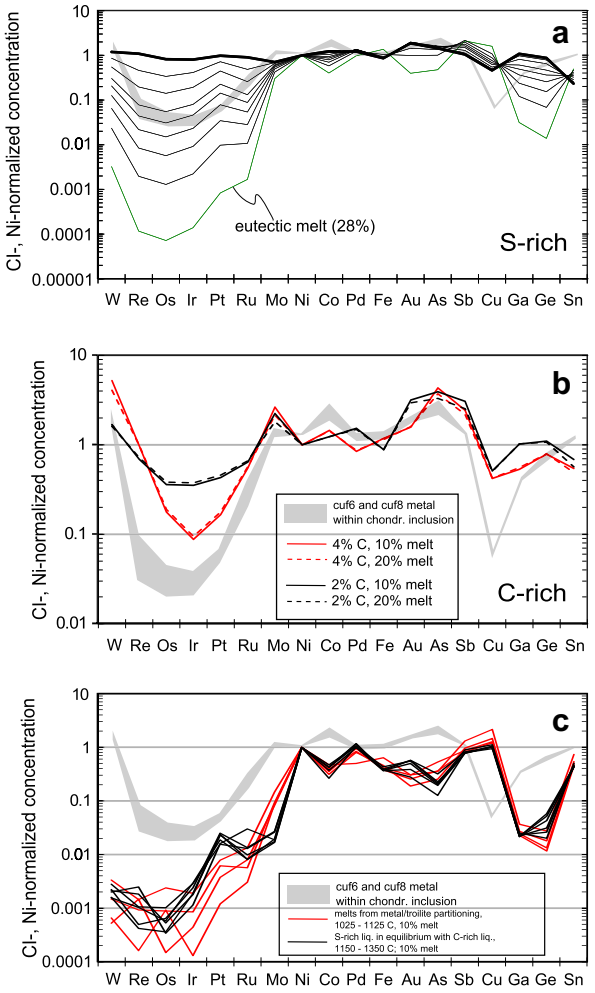

Fig. 8. CI-, Ni-normalized siderophile element patterns for model patterns of liquid metal/solid metal differentiation. Batch partial melting of an enstatite chondrite metal (Kong et al., 1997) was modeled with experimentally determined partition coefficients for S- and C-rich melts. (a) S-rich melt composition, partition parameters D_0 and β from Chabot and Jones (2003) and Chabot et al. (2003, 2009; see Table 4 for details) with 5% increments in the degree of melting beginning at the Fe–FeS eutectic; (b) C-rich melt composition, partition coefficients D from Chabot et al. (2006, experiments C16 and C6; 2008, experiments A174 and A421, see Table 4 for details) black 2% C, red 4% C, solid lines 10% partial melt, dashed lines 20% partial melt; (c) graphite-saturated Fe–S melts, temperature range from 1025 to 1350 °C, 10% partial melt; partition coefficients from Hayden et al. (2011) and Chabot et al. (Ga, Sb, Sn, 2003; 2009). Red lines: Fe–S melts in a C-saturated system, 1025–1125 C, black lines, S-rich metallic liquids in equilibrium with C-rich metallic liquids, 1150–1350 C. For the partition coefficients used, see Table 3 in Hayden et al. (2011). Gray shaded field in (a)–(c): fractionated patterns from Cumberland Falls. Concentrations for CI chondrite taken from Table 2. (For interpretation of the references to color in this figure legend, the reader is referred to the web version of this article.)

vation from either EL or EH metal as parental material (Fig. 2b and c). The other, more volatile siderophile elements (Ga, Ge, and Sn), show distinct differences in their normalized patterns between Mt. Egerton and aubrites

sensu stricto. In contrast to Mt. Egerton, Sn, the most volatile siderophile element analyzed in this study, is enriched compared to less volatile elements such as Ge and Ga (Fig. 5a). Tin is also more incompatible than Ga and Ge (Fig. 8). This enrichment in Sn is common to metal in three different aubrite samples. Aubrites thus seem to have quenched metallic liquid with high Sn contents, whereas Mt. Egerton may contain solid metal depleted in Sn relative to Ga and Ge.

Cumberland Falls section USNM 477-1 has previously been studied in detail by Neal and Lipschutz (1981), who described a large part of this section as a chondritic inclusion (Fig 1b). Interestingly, the two most compatible HSE-depleted grains cuf6 and cuf8, as well as the sulfide cuf5 (highly siderophile elements below the detection limit), are from within this chondritic inclusion, whereas the non- or moderately depleted grains cuf3 and cuf4 were sampled outside of the inclusion (Fig 1b). The depleted metal grains in Aubres are not associated with chondritic inclusions. The volatile part of the siderophile element pattern is virtually identical between metal from the aubrite breccias and that from the chondritic inclusions. The depletion of compatible HSE Re, Os, Ir, Ru, and Pt in metals within the chondritic inclusion in Cumberland Falls to values of 0.02–0.03 times CI is similar, albeit more pronounced, to the depletion of 0.15–0.5 times CI noted in kamacite from the EL3 chondrite Pecora Escarpment 91020 by van Niekerk et al. (2009) (Fig 7). Removal of S- and C- rich liquid metal upon crystallization of metallic liquid could produce the observed depletions, because the compatible HSE Os, Re, Ir, and Pt all partition into solid metal over liquid metal (Jones and Drake, 1983; Chabot and Drake, 2000; Chabot et al., 2003, 2006, 2008; Corrigan et al., 2009). The formation of such melt from enstatite chondrite metal was attributed to impact melting and injection of liquid metal into the meteorite protolith, potentially after fractional crystallization during migration, based on the absence of complementary, enriched siderophile element patterns (van Niekerk et al., 2009).

4.2.1. Modeling the siderophile element variation in aubrites

van Niekerk et al. (2009) showed that addition of partial melts containing both C-rich and S-rich metallic liquids derived from impact melting of E chondrites could explain the siderophile element patterns observed in EL3 PCA 91020 metal. While impact melting or short, non-equilibrium melting has been suggested for the origin of Mayo Belwa, Pena Blanca Spring and inclusions in Cumberland Falls based on petrography and REE signatures of oldhamite (Lodders et al., 1993; Rubin, 2010), it has not been identified in the majority of aubrites. The basic chemical differentiation observed in fractionated, strongly non-chondritic siderophile element patterns is similar between low grade enstatite chondrites and achondrites (Fig. 7). Melting of enstatite chondrite metal and subsequent isolation from the solid phase was modeled using the equations derived by Shaw (1970) for both fractional and batch melting with EH and EL type bulk metal (Kong et al., 1997) as the starting material. Because model results from EH and EL metal, as well as batch and fractional melting models have only minor differences that do not affect the conclusions drawn, the discussion is limited to batch melting of EL type metal.

Results of the modeling are shown as CI–Ni normalized patterns in Fig 8. The average siderophile element composition of EL metal from Kong et al. (1997) was used as the starting material. Partition coefficients used for the modeling of S-rich metals were calculated with the parameterization model developed by Chabot and Jones (2003), and with parameters from Chabot et al. (2003, 2009). Partition coefficients for modeling of C-rich melts were taken from Chabot et al. (2006; experiments C12 and C16; 2008, experiments A174 and A421). Copper was parameterized linearly with S content (Chabot et al., 2009). Starting material composition for Sn was estimated using the enstatite chondrite average from Wasson and Kallemeyn (1988).

Pressure is difficult to constrain for aubrites, due to the unknown size of the parent body and the exotic mineral composition, rendering common geobarometers unusable. Assuming a parent body with internal pressures less than 5 GPa (Zellner et al., 1977), the pressure effect on siderophile partitioning is small (Chabot et al., 2008, 2011), and is not considered for the model. Similarly, the effect of Si content in metal is not taken into account here because of the low Si concentrations present in aubrite metal (Table 1), and the fact that Si fractionation effects are small compared to those caused by C and S (Chabot et al., 2010).

Batch melting of both S-rich and C-rich parent material can each reproduce a subset of the observed features of siderophile element patterns in enstatite achondrite metals (Fig. 8). However, both models have significant differences from the patterns observed in the metal of the Cumberland Falls chondrite inclusion. Patterns of the melts obtained by modeling at small degrees of melting near the eutectic of S-rich metal reproduce some of the observed patterns in aubrite metal, notably the depletion in compatible HSE of one to three orders of magnitude and the comparatively flat pattern for moderately volatile elements of Mo to Au. With increasing degrees of melting, the patterns flatten out to approach the starting material chondrite composition (Fig. 8a).

Carbon-rich melts show higher W/Re ratios than S-rich melts, and better reproduce the observed fractionation of Ru from Pt and Ir, the mild enrichment of As over Au and upward trending patterns for the most volatile elements of Cu to Ge. However, C-rich metallic liquids produce stronger Re/Os fractionation compared to S-rich metallic liquids, and compared to the aubrite HSE patterns (Figs. 5, 7 and 8). Even the most extreme depletion of compatible HSE in models with small degrees of C-rich composition is 0.5–1 orders of magnitude less than that observed in Cumberland Falls metal, and about two orders of magnitude less than that observed in Aubres metal. For C-rich compositions, there is little difference in elements from Mo through Sn for models with either 2% or 4% C content and 10% or 20% degree of partial melting. There is substantial difference in the compatible HSE, which are depleted by about half an order of magnitude more for the 4% C composition, but not significantly affected by degree of melting (Fig. 8b).

A recent study by Hayden et al. (2011) studied siderophile element partitioning in a C-saturated Fe–S system.

Under pressures less than ~5–6 GPa, immiscible liquid alloys coexist in the Fe–C–S system above ~1150 °C (Raghavan, 1988; Corgne et al., 2008; Dasgupta et al., 2009). These results on liquid metal immiscibility could be applicable to the history of aubrites as tested below.

Differences between partitioning in the solid metal/liquid S-rich metal (at lower temperature up to ~1150 °C) and liquid C-rich metal/liquid S-rich metal (at higher temperature above 1150 °C) are minor (Hayden et al., 2011), with the exception of refractory elements W through Mo. The experimentally determined partition coefficients show scatter, coupled with significant uncertainties especially towards the lower end of the studied temperature range (Hayden et al., 2011). A significant influence of C on trace element partitioning was found when compared to the pure Fe–S system (Hayden et al., 2011), notably in W, the compatible HSE, Mo, As, and Au, all of which partition more strongly into the C-rich liquid compared to C-free Fe–S systems (Chabot et al., 2009; Hayden et al., 2011). Results of modeling of both high and low temperature partitioning in the Fe–C–S system analogous to the Fe–C system are shown in Fig. 8c. These model results using the parameters of Hayden et al. (2011) do not present a good fit to the patterns observed in Cumberland Falls and Aubres metal. Resulting melt patterns show depletion by up to 3 orders of magnitude in refractory elements (W, Re, Os, Ir, Pt, Ru, Mo) as well as in Ga and Ge, while recording depletion of up to 50% in other siderophile elements (Fig. 8c), as well as slight enrichments in Pd and Cu.

As with modeling in the Fe–S system, depletions in compatible HSE are more pronounced in the model calculation than observed in aubrites. The high W/Re, positive anomalies in Co, and negative anomalies in Cu seen in patterns from Cumberland Falls and Aubres cannot be reproduced.

To reduce the discrepancies between models and observation, the minor element compositions of the parental metallic liquids may need to be adjusted, and intermediate compositions containing both substantial amounts of S and C may be required to produce observed aubrite metal compositions by partial melting of enstatite chondrite metal. It is difficult to estimate the relative proportions of S-rich and C-rich metal in the original parental metal. Moreover, the effects of metal compositions on siderophile trace element solid metal/liquid metal behavior are likely different for each element, and potentially interdependent (Jana and Walker, 1997a,b; Chabot et al., 2006, 2008, 2010; Hayden et al., 2011). Depletion in compatible HSE of one to three orders of magnitude (Figs. 2, 5 and 7) requires a substantial S content above 5%, but lower than the 25–29 wt.% used in the most S-rich experiments of Chabot et al. (2003) and Hayden et al. (2011). The same applies to the C contents, which need to be moderately high (>2%) but lower than the 3.6% used by Chabot et al. (2006).

In summary, melting models in the Fe–S and Fe–C system suggest that the metal compositions of the aubrites Cumberland Falls and Aubres can potentially be derived from partial melting of either EL or EH chondrite metal and subsequent isolation of the solid portion, assuming that the liquid metal phase contains both S and C. In contrast, modeling using the results of melting experiments in a C-saturated Fe–S system with immiscible Fe–S and Fe–C melts does not reproduce the observed siderophile element patterns of aubrites. Immiscibility of S-rich and C-rich metallic liquids thus does not appear to play a major role in the formation history of aubrites.

4.2.2. A common origin for enstatite chondrites and achondrites?

A genetic relationship between enstatite chondrites and enstatite achondrites (including aubrites) is consistent with their identical oxygen isotope compositions, supporting derivation from a similar nebular reservoir (Clayton et al., 1984; Clayton and Mayeda, 1996). Some previous petrological and geochemical studies have also concluded that aubrites were derived by igneous processes from enstatite chondrite parental material (Watters and Prinz, 1979; Wolf et al., 1983). Siderophile element systematics in metals in aubrites and anomalous enstatite meteorites provide several indications for a shared origin with enstatite chondrites. Four out of five metal grains in Mt. Egerton and one in Mayo Belwa have nearly unfractionated siderophile element patterns that are very similar to EL or EH bulk metal patterns (Kong et al., 1997) (Figs. 2 and 5b). This is consistent with a genetic link to EL and EH chondrites with little or no solid metal/liquid metal differentiation in the fractions measured in these meteorites. Trace element modeling of the new siderophile element data for enstatite achondrites shows that fractionated siderophile element patterns in Mt. Egerton, Aubres or Cumberland Falls can be generated from liquid metal/solid metal differentiation from enstatite chondrite metal (Figs. 5 and 8). Furthermore, fractionated siderophile element patterns in aubrite metals bear similarity to patterns in metal from EL3 chondrite PCA 91020 (van Niekerk et al., 2009; Fig. 7). Siderophile element patterns in aubrites are thus consistent with a derivation of aubrites from enstatite chondrites by planetary differentiation processes, possibly on a different, but compositionally similar body.

A common origin of aubrites and E chondrites is in contrast to some past studies which concluded that aubrites could not have been generated from either EL or EH chondrites (Richter et al., 1979; Easton, 1986; Brett and Keil, 1986; Keil, 1989). It should be noted that some of the original arguments against an igneous origin of aubrites (Richter et al., 1979) have been overturned by subsequent expanded studies by the same group (Wolf et al., 1983). Among the issues with a formation of aubrites from enstatite chondritic material is the high Ti concentration in troilite in aubrites (Keil, 1989), although several samples from this study show troilite Ti concentrations of <1%, closer to enstatite chondrites (Table 1; Shallowater, ALH 84007, Cumberland Falls). Alternatively, Ti concentration in troilite can be increased by loss of S to basaltic liquid (Fogel, 1997), or increased Ti partitioning into troilite during melting of EL lithologies, as suggested for a clast from EL6 Hvittis, which contains troilite with 2.5 wt.% Ti (Rubin, 1983).

The presence of up to 8% of diopside in aubrites (Lonsdale, 1947; Hey and Easton, 1967; Watters and Prinz, 1979; Okada et al., 1988), compared to minor occurrence in only

a few enstatite chondrites (Keil, 1989), and the required size of the parent body to generate pressure high enough to crystallize forsterite (Fogel et al., 1988; Keil, 1989) are inconsistent with an origin of aubrites by differentiation of known enstatite chondrites (see Mittlefehldt et al., 1998, for the opposite point of view). Thus, while siderophile element and oxygen isotope data are consistent with a common origin, petrological considerations as well as geochemical data from sulfides and silicates imply otherwise. A new physical model of differentiated asteroids with chondritic crusts (Elkins-Tanton et al., 2011) re-opens the issue of whether aubrites or differentiated enstatite achondrites may also originate on the same parent body. Thus, siderophile element and oxygen isotope data may be better interpreted as evidence of formation of enstatite achondrites by melting of material derived from the same reservoir from which enstatite chondrites formed, they do not yet provide definitive evidence for formation on the same parent body. Combined with additional studies on the silicate and sulfide components of known aubrites, such evidence may ultimately be obtained from finding new meteorites (primitive enstatite meteorites transitional between chondrites and achondrites, e.g. Queen Alexandra Range 94204; Izawa et al., 2011) or from future sample recovery from E asteroids.

4.2.3. Origin of Cumberland Falls inclusions

Prior to the advent of the present day meteorite nomenclature, the Cumberland Falls chondritic inclusions have been described as 'forsterite chondrites' (Graham et al., 1977). Based on uniform Mg/Si ratios of 0.95, similar mineralogy (low-Fa olivine, high-Cr troilite, and low-Ca pyroxene) and oxidation state similar to ordinary chondrites, Cumberland Falls inclusions were initially suggested to be related by crystal/liquid fractionation to the meteorites Kakangari, Winona, Mount Morris (Wisconsin) and Pontlyfni (Graham et al., 1977). Upon revision, these meteorites were reclassified either as K chondrites (for Kakangari) or Winonaites (e.g. Weisberg et al., 1996; Benedix et al., 1998). A recent study interprets the inclusions as fragments of an LL ordinary chondrite impactor based on textural analysis (Rubin, 2010), with some inclusions representing impact melt breccias. Highly siderophile element patterns in metal within the inclusion (cuf6, cuf8) are compatible HSE depleted (Fig. 5a), and are broadly similar to patterns from PCA 91020 (Fig. 7). However, they are different from patterns seen in LL4 Soko-Banja (Campbell and Humayun, 2003), which show no pronounced depletion in the siderophile elements considered (Mo, Ru, Pd, W, Re, Os, Ir, Pt, Au), and HSE concentrations of which are about an order of magnitude greater than those in Cumberland Falls. The absence of complementary, compatible HSE-enriched patterns in both Cumberland Falls inclusions and EL3 chondrite PCA 91020 suggests injection of the metallic liquid into the protolith rock on their respective parent bodies, in accordance with models suggested by Rubin (2010). In order to determine the origin of these chondritic inclusions in more detail, additional siderophile element analyses of ordinary chondrites, K chondrites, and winonaites are required.

4.3. Shallowater

Shallowater section USNM 1206-2 is different from all other sections examined in the course of this study, as it contains no metal, in contrast to the majority of studied specimens and sections from Shallowater with up to 10% of metal (Foshag, 1940; Wasson and Wai, 1970; Watters and Prinz, 1979; Keil et al., 1989). If metal/sulfide equilibrium occurred, the troilites studied in USNM 1206-2 should yield similar siderophile element concentrations to sulfides from other aubrites (e.g. cuf5). This is indeed the case for most elements, with the exception of Cu, Zn, V, and Nb, which are considerably more enriched in Shallowater troilite compared to sulfides in other aubrites studied (Table 2, Fig 5c, Supplemental Table 2). Comparison of HSE concentrations in sulfides between Shallowater and other aubrites is rendered more difficult by concentrations of HSE in sulfides from aubrites other than Shallowater being below the detection limit (Supplemental Table 2).

As in Cumberland Falls and Aubres metal, Os in Shallowater troilite is depleted compared to Re by over an order of magnitude (Fig. 5). This depletion is far greater than that predicted by models of crystallization of metal from Fe–S or Fe–C liquids (Fig. 8), and opposite to observations from bulk rock measurements, which have Re/Os values of ~0.5 chondritic (van Acken et al., 2011). While for Shallowater, this unexpected fractionation could be explained by a missing Os–Ir–Pt-rich metal phase, there is no satisfactory explanation for the divergence between model and observation for Cumberland Falls or Aubres metal. Alternatively, studies of IAB irons Canyon Diablo and Odessa showed elevated Re/Os in troilite over metal, which was attributed to recent open system behavior (Shen et al., 1996). Because of the differences in Re and Os concentration between coexisting sulfides and metals in these samples of about three orders of magnitude, no effect on the Re–Os signatures in metal is expected despite the fractionated signatures in troilite (Shen et al., 1996).

Modeling the history of Shallowater and comparison to the aubrites and Mt. Egerton is thus difficult. Metal seems to have played an important part in the formation history of the Shallowater parent body, potentially even by formation and differentiation of a small core (Keil et al., 1989). Based on the cooling history derived from enstatite and kamacite petrography and geochemistry, Keil et al. (1989) suggested a complex multistage history for Shallowater with destruction of a differentiated parental body by impact followed by gravitational reassembly. The high Ni contents in troilite found by Keil et al. (1989) are mostly confirmed (0.18% vs. 0.25%), potentially reducing the annealing and equilibration temperature suggested by Keil et al. (1989) from 700 to 650 °C. High Ti, Mn, and Cr contents (Keil et al., 1989; Table 1) are also confirmed.

5. CONCLUSIONS

Enstatite achondrite sulfides and metals record a complex history of planetary differentiation events. Their siderophile element signatures are consistent with multiple parent bodies, and are best explained by variable degrees

of melt extraction and differentiation, asteroid break-up and re-accretion, with some aubrites probably recording infiltration by impact melts. Siderophile element signatures from Mt. Egerton metals are consistent with crystallization from metallic liquids complementary to another anomalous enstatite achondrite, NWA 2526 (Humayun et al., 2009). This complementarity between the metal composition of NWA 2526 and that of Mt. Egerton potentially constrain a common origin of these two meteorites on an E-chondrite-like parent body (Keil and Bischoff, 2008).

Metals and sulfides from Cumberland Falls, Aubres, and Shallowater show various degrees of depletion in compatible siderophile elements, consistent with S- and C-rich liquid metal at low to moderate degrees of partial melting during planetary differentiation of enstatite chondrite-like parent bodies. Both S- and C-rich metal liquids can partially reproduce the siderophile element patterns observed in Cumberland Falls and Aubres, while removal of a hybrid S-C-containing metallic liquid might reproduce their features more closely. In order to produce the observed siderophile element patterns in metals after removal of >10% of metallic liquid, required light element contents are estimated at >5% S and >2% C. However, models using partition coefficients obtained for a graphite saturated Fe–S system taking liquid immiscibility in the Fe–S–C system into account fail to replicate the patterns observed in aubrite metals. Impact melting, as suggested previously for both EL chondrites (van Niekerk et al., 2009) and aubrites (Rubin, 2010), followed by infiltration of the impact-generated melts into the precursor rock of the respective meteorite on the parent body, may be a viable process to generate the observed signatures.

Associations of metal, phosphide, and Mg-rich alabandite in Mt. Egerton allow estimates for siderophile element partitioning between these phases under the reduced conditions during enstatite meteorite formation. The HSE and a number of other elements (Ga, Ge, As, Sb) show preference for metal and phosphide, while Ni and Mo are strongly concentrated in the phosphide. Nominally lithophile elements (e.g. V, Mn, Sr, Y, Zr, Nb) were not detected in the metal, but show some affinity for both phosphide and sulfide.

The findings from this study are consistent with a genetic link between enstatite chondrites and aubrites, as siderophile element patterns in aubrite metals are either similar to those found in enstatite chondrites (Kong et al., 1997, Fig. 2), or can be generated by partial melting of enstatite chondrite metal. This conclusion assumes moderate contents of S and C in the parental metal (Fig. 8). However, siderophile element patterns in aubrite metals also underscore the heterogeneity present within the aubrite meteorites. While an origin of aubrites on multiple differentiated planetary bodies, including those previously labeled as APB and the parent body of Shallowater (Keil et al., 1989) cannot be ruled out, a potential origin of some aubrites and enstatite chondrites on a single parent body must be considered in view of recent models for formation of carbonaceous chondrites proposed by Elkins-Tanton et al. (2011). Models of parent body breakup and reassembly (Keil, 1989) or extensive impact melting (Rubin, 2010) can be neither contradicted nor confirmed, although the heterogeneity in different parts from the polymict aubrite breccias Cumberland Falls (Figs. 1 and 5a) and the similarity to impact melts in EL3 PCA 91020 (van Niekerk et al., 2009; Fig. 7) support these notions.

ACKNOWLEDGEMENTS

Sections used in this study were provided by the National Museum of Natural History (Smithsonian Institution: Aubres, Mayo Belwa, Cumberland Falls, Shallowater, Mount Egerton, Bishopville, Khor Temiki, Norton County) and by the Meteorite Working Group at Lyndon B. Johnson Space Center (ALH 84007, LAP 03719). This research was supported by the NASA Cosmochemistry program via grants NNX09AG87G and NNX10AI37G to M.H. and RTOP 344-31-72-06 and NNX10AB37G to A.D.B. D.v.A. was supported by a postdoctoral fellowship through the ORAU NPP program, and by internal support through the University of Houston. Reviews by A. Rubin, N. Chabot, R. Ash, and an anonymous reviewer, as well as editorial comments by R.J. Walker, greatly improved the manuscript. We acknowledge technical assistance from D.K. Ross.

APPENDIX A. SUPPLEMENTARY DATA

Supplementary data associated with this article can be found, in the online version, at doi:10.1016/j.gca.2011.12.025.

REFERENCES

Anders E. and Grevesse N. (1989) Abundances of the elements: meteoritic and solar. *Geochim. Cosmochim. Acta* **53**, 197–214.

Benedix G. K., McCoy T. J., Keil K., Bogard D. D. and Garrison D. H. (1998) A petrologic and isotopic study of winonaites: evidence for early partial melting, brecciation, and metamorphism. *Geochim. Cosmochim. Acta* **62**(14), 2535–2553.

Borisov A. and Palme H. (1997) Experimental determination of the solubility of platinum in silicate melts. *Geochim. Cosmochim. Acta* **61**(20), 4349–4357.

Borisov A., Palme H. and Spettel B. (1994) Solubility of palladium in silicate melts – implications for core formation in the Earth. *Geochim. Cosmochim. Acta* **58**(2), 705–716.

Brenan J. M. and McDonough W. F. (2009) Core formation and metal–silicate fractionation of osmium and iridium from gold. *Nat. Geosci.* **2**(11), 798–801.

Brett R. and Keil K. (1986) Enstatite chondrites and enstatite achondrites (aubrites) were not derived from the same parent body. *Earth Planet. Sci. Lett.* **81**, 1–6.

Campbell A. J. and Humayun M. (2003) Formation of metal in Grosvenor mountains 95551 and comparison to ordinary chondrites. *Geochim. Cosmochim. Acta* **67**(13), 2481–2495.

Campbell A. J., Humayun M., Meibom A., Krot A. N. and Keil K. (2001) Origin of zoned metal grains in the QUE94411 chondrite. *Geochim. Cosmochim. Acta* **65**(1), 163–180.

Campbell A. J., Humayun M. and Weisberg M. K. (2002) Siderophile element constraints on the formation on metal in the metal-rich chondrites Bencubbin, Weatherford, and Gujba. *Geochim. Cosmochim. Acta* **66**(4), 647–660.

Campbell A. J., Simon S. B., Humayun M. and Grossman L. (2003) Chemical evolution of metal in refractory inclusions in CV3 chondrites. *Geochim. Cosmochim. Acta* **67**, 3119–3134.

Capobianco C. J., Drake M. J. and De'Aro J. (1999) Siderophile geochemistry of Ga, Ge, and Sn: cationic oxidation states in silicate melts and the effect of composition in iron–nickel alloys. *Geochim. Cosmochim. Acta* **63**(17), 2667–2677.

Casanova I., Keil K. and Newsom H. E. (1993) Composition of metal in aubrites: constraints on core formation. *Geochim. Cosmochim. Acta* **57**, 675–682.

Chabot N. L. and Drake M. J. (2000) Crystallization of magmatic iron meteorites: the effects of phosphorus and liquid immiscibility. *Meteorit. Planet. Sci.* **35**, 807–816.

Chabot N. L. and Jones J. H. (2003) The parametrization of solid metal – liquid metal partitioning of siderophile elements. *Meteorit. Planet. Sci.* **38**(10), 1425–1436.

Chabot N. L., Campbell A. J., Jones J. H., Humayun M. and Agee C. B. (2003) An experimental test of Henry's Law in solid metal – liquid metal systems with implications for iron meteorites. *Meteorit. Planet. Sci.* **38**(2), 181–196.

Chabot N. L., Campbell A. J., Jones J. H., Humayun M. and Lauer, Jr, H. V. (2006) The influence of carbon on trace element partitioning behavior. *Geochim. Cosmochim. Acta* **70**, 1322–1335.

Chabot N. L., Campbell A. J., McDonough W. F., Draper D. S., Agee C. B., Humayun M., Watson H. C., Cottrell E. and Saslow S. A. (2008) The Fe–C system at 5 GPa and implications for Earth's core. *Geochim. Cosmochim. Acta* **72**, 4146–4158.

Chabot N. L., Saslow S. A., McDonough W. F. and Jones J. H. (2009) An investigation of the behavior of Cu and Cr during iron meteorite crystallization. *Meteorit. Planet. Sci* **44**(4), 505–519.

Chabot N. L., Safko T. M. and McDonough W. F. (2010) Effect of silicon on trace element partitioning in iron-bearing metallic melts. *Meteorit. Planet. Sci.* **45**(8), 1243–1257.

Chabot N. L., McDonough W. F., Jones J. H., Saslow S. A., Ash R. D., Draper D. S. and Agee C. B. (2011) Partitioning behavior at 9 GPa in the Fe–S system and implications for planetary evolution. *Earth Planet. Sci. Lett.* **305**(3–4), 425–434.

Clayton R. N. and Mayeda T. K. (1996) Oxygen isotope studies of achondrites. *Geochim. Cosmochim. Acta* **60**(11), 1999–2017.

Clayton R. N., Mayeda T. K. and Rubin A. E. (1984) Oxygen isotopic composition of enstatite chondrites and aubrites. *J. Geophys. Res.* **89**(Supplement), C245–C249.

Cook D. L., Humayun M., and Campbell A. J. (2004) The distribution of molybdenum in the Indarch EH4 chondrite. *35th Lunar and Planet. Sci. Conf*. #1163 (abstr.).

Corgne A., Wood B. J. and Fei Y. (2008) C- and S-rich molten alloy immiscibility and core formation of planetesimals. *Geochim. Cosmochim. Acta.* **72**(9), 2409–2416.

Corrigan C. M., Chabot N. L., McCoy T. J., McDonough W. F., Watson H. C., Saslow S. A. and Ash R. D. (2009) The iron–nickel–phosphorus system: effects on the distribution of trace elements during the evolution of iron meteorites. *Geochim. Cosmochim. Acta* **73**, 2674–2691.

Crozaz G. and Lundberg L. L. (1995) The origin of oldhamite in unequilibrated enstatite chondrites. *Geochim. Cosmochim. Acta* **59**(18), 3817–3831.

Dasgupta R., Buono A., Whelan G. and Walker D. (2009) High-pressure melting relations in Fe–C–S systems: implications for formation, evolution, and structure of metallic cores in planetary bodies. *Geochim. Cosmochim. Acta* **73**, 6678–6691.

Dickinson T. L. and McCoy T. J. (1997) Experimental rare-earth-element partitioning in oldhamite: implications for the igneous origin of aubritic oldhamite. *Meteorit. Planet. Sci.* **32**, 395–412.

Easton A. J. (1986) Studies of kamacite, perryite and schreibersite in E-chondrites and aubrites. *Meteoritics* **21**(1), 79–93.

Elkins-Tanton L. T., Weiss B. P. and Zuber M. T. (2011) Chondrites as samples of differentiated planetesimals. *Earth Planet. Sci. Lett.* **305**(1–2), 1–10.

Fischer-Gödde M., Becker H. and Wombacher F. (2010) Rhodium, gold and other highly siderophile element abundances in chondritic meteorites. *Geochim. Cosmochim. Acta* **74**, 356–379.

Floss C. and Crozaz G. (1993) Heterogeneous REE patterns in oldhamite from aubrites: their nature and origin. *Geochim. Cosmochim. Acta* **57**, 4039–4057.

Floss C., Strait M. M. and Crozaz G. (1990) Rare earth elements and the petrogenesis of aubrites. *Geochim. Cosmochim. Acta* **54**, 3553–3558.

Fogel R. A. (1997) The enstatite chondrite-achondrite link reforged: solution of the titanium in troilite problem. *Meteorit. Planet. Sci.* **32**(4), A43.

Fogel R. A., Hess P. C. and Rutherford M. J. (1988) The enstatite chondrite–achondrite link. *19th Lunar and Planet. Sci. Conf.*, 342–343.

Foshag W. F. (1940) The Shallowater meteorite: a new aubrite. *Am. Min.* **25**, 779–786.

Gaboardi M. and Humayun M. (2009) Elemental fractionation during LA-ICP-MS analysis of silicate glasses: implications for matrix-independent standardization. *J. Anal. At. Spectrom.* **24**(9), 1188–1197.

Graham A. L. (1978) Metal and schreibersite in Mayo Belwa, an enstatite achondrite. *Meteoritics* **13**(2), 235–244.

Graham A. L. and Hendersonm P. (1985) Rare earth element abundances in separated phases of Mayo Belwa, an enstatite achondrite. *Meteoritics* **20**(1), 141–149.

Graham A. L., Easton A. J. and Hutchison R. (1977) Forsterite chondrites; the meteorites Kakangari, Mount Morris (Wisconsin), Pontlyfni, and Winona. *Mineral. Mag.* **41**, 201–210.

Hayden L. A., Van Orman J. A., McDonough W. F., Ash R. D. and Goodrich C. A. (2011) Trace element partitioning in the Fe–S–C system and its implications for planetary differentiation and the thermal history of ureilites. *Geochim. Cosmochim. Acta* **75**(21), 6570–6583.

Hey M. H. and Easton A. J. (1967) The Khor Temiki meteorite. *Geochim. Cosmochim. Acta* **31**, 1789–1792.

Holzheid A., Sylvester P., O'Neill H. S. C., Rubie D. C. and Palme H. (2000) Evidence for a late chondritic veneer in the Earth's mantle from high-pressure partitioning of palladium and platinum. *Nature* **406**, 396–399.

Horan M. F., Walker R. J., Morgan J. W., Grossman J. N. and Rubin A. E. (2003) Highly siderophile elements in chondrites. *Chem. Geol.* **196**, 5–20.

Hsu W. and Crozaz G. (1998) Mineral chemistry and the origin of enstatite in unequilibrated enstatite chondrites. *Geochim. Cosmochim. Acta* **62**(11), 1993–2004.

Humayun M., Simon S. B. and Grossman L. (2007) Tungsten and hafnium distribution in calcium–aluminum inclusions (CAIs) from Allende and Efremovka. *Geochim. Cosmochim. Acta* **71**, 4609–4627.

Humayun M., Keil K., and Bischoff A. (2009) Siderophile elements in metal from Northwest Africa 2526, an enstatite chondrite partial melt residue. *40th Lunar and Planet. Sci. Conf.* #1744 (abstr.).

Humayun M., Davis F. A. and Hirschmann M. M. (2010) Major element analysis of natural silicates by laser ablation ICP-MS. *J. Anal. At. Spectrom.* **25**, 998–1005, doi: 10.1039/C001391A.

Izawa M. R. M., Flemming R. L., Banerjee N. R. and Matveev S. (2011) QUE 94204: a primitive enstatite achondrite produced by the partial melting of an E chondrite-like protolith. *Meteorit. Planet. Sci.* **46**(11), 1742–1753.

Jana D. and Walker D. (1997a) The influence of sulfur on partitioning of siderophile elements. *Geochim. Cosmochim. Acta* **61**(24), 5255–5277.

Jana D. and Walker D. (1997b) The impact of carbon on element distribution during core formation. *Geochim. Cosmochim. Acta* **61**(13), 2759–2763.

Jana D. and Walker D. (1997c) The influence of silicate melt composition on distribution of siderophile elements among metal and silicate liquids. *Earth Planet. Sci. Lett.* **150**, 463–472.

Jochum K. P., Stoll B., Herwig K., Willbold M., Hofmann A. W., Amini M., Aarburg S., Abouchami W., Hellebrand E., Mocek B., Raczek I., Stracke A., Alard O., Bouman C., Becker S., Ducking M., Bratz H., Klemd R., de Bruin D., Canil D., Cornell D., de Hoog C. J., Dalpe C., Danyushevsky L., Eisenhauer A., Gao Y. J., Snow J. E., Goschopf N., Günther D., Latkoczy C., Guillong M., Hauri E. H., Hofer H. E., Lahaye Y., Horz K., Jacob D. E., Kasemann S. A., Kent A. J. R., Ludwig T., Zack T., Mason P. R. D., Meixner A., Rosner M., Misawa K. J., Nash B. P., Pfander J., Premo W. R., Sun W. D., Tiepolo M., Vannucci R., Vennemann T., Wayne D. and Woodhead J. D. (2006) MPI-DING reference glasses for in situ microanalysis: new reference values for element concentrations and isotope ratios. *Geochem. Geophys. Geosyst.* **7**, 89–90, doi: 10.1029/2005GC001060.

Jones J. H. and Drake M. J. (1983) Experimental investigations of trace element fractionation in iron meteorites, II: The influence of sulfur. *Geochim. Cosmochim. Acta* **47**, 1199–1209.

Jones J. H. and Malvin D. J. (1990) A nonmetal interaction-model for the segregation of trace-metals during solidification of Fe–Ni–S, Fe–Ni–P, and Fe–Ni–S–P alloys. *Metall. Trans. B* **21**(4), 697–706.

Keil K. (1969) Titanum distribution in enstatite chondrites and achondrites, and its bearing on their origin. *Earth Planet. Sci. Lett.* **7**, 243–248.

Keil K. (1989) Enstatite meteorites and their parent bodies. *Meteoritics* **24**, 195–208.

Keil K. (2010) Enstatite achondrite meteorites (aubrites) and the histories of their asteroidal parent bodies. *Chem. Erde* **70**(4), 295–317.

Keil K. and Bischoff A. (2008) Northwest Africa 2526: a partial melt residue of enstatite chondrite parentage. *Meteorit. Planet. Sci.* **43**(7), 1233–1240.

Keil K. and Fredriksson K. (1963) Electron microprobe analysis of some rare minerals in the Norton County achondrite. *Geochim. Cosmochim. Acta* **27**, 939–947.

Keil K., Ntaflos T., Taylor G. J., Brearley A. J., Newsom H. E. and Romig, Jr., A. D. (1989) The Shallowater aubrite: evidence for origin by planetesimal impacts. *Geochim. Cosmochim. Acta* **53**, 3291–3307.

Kong P., Mori T. and Ebihara M. (1997) Compositional continuity of enstatite chondites and implications for heterogeneous accretion of the enstatite chondrite parent body. *Geochim. Cosmochim. Acta* **61**(22), 4895–4914.

Li J. and Agee C. B. (1996) Geochemistry of mantle-core differentiation at high pressure. *Nature* **381**(6584), 686–689.

Li J. and Agee C. B. (2001) The effect of pressure, temperature, oxygen fugacity and composition on partitioning of nickel and cobalt between liquid Fe–Ni–S alloy and liquid silicate: implications for the Earth's core formation. *Geochim. Cosmochim. Acta* **65**(11), 1821–1832.

Lodders K. (1996) An experimental and theoretical study of rare-earth-element partitioning between sulfides (FeS, CaS) and silicate and applications to enstatite achondrites. *Meteorit. Planet. Sci.* **31**, 749–766.

Lodders K. (2003) Solar system abundances and condensation temperatures of the elements. *Astrophys. J.* **591**, 1220–1247.

Lodders K., Palme H. and Wlotzka F. (1993) Trace elements in mineral separates of the Pena Blanca Spring aubrite: implications for the evolution of the aubrite parent body. *Meteoritics* **28**, 538–551.

Lonsdale J. T. (1947) The Pena Blanca Spring meteorite, Brewster County, Texas. *Am. Min.* **32**, 354–364.

Malvin D. J., Jones J. H. and Drake M. J. (1986) Experimental investigations of trace-element fractionation in iron-meteorites. 3. Elemental partitioning in the system Fe–Ni–S–P. *Geochim. Cosmochim. Acta* **50**(6), 1221–1231.

Mann U., Frost D. J. and Rubie D. C. (2009) Evidence for high-pressure core-mantle differentiation from the metal–silicate partitioning of lithophile and weakly siderophile elements. *Geochim. Cosmochim. Acta* **73**, 7360–7386.

Mittlefehldt D. W., McCoy T. J., Goodrich C. A. and Kracher A. (1998) Non-chondritic meteorites from asteroidal bodies. In *Reviews in Mineralogy, Vol. 36: Planetary Materials* (ed. J. J. Papike). Mineralogical Society of America, pp. 4-1–4-195.

Neal C. W. and Lipschutz M. E. (1981) Cumberland Falls chondritic inclusions: mineralogy/petrology of a forsterite chondrite suite. *Geochim. Cosmochim. Acta* **45**, 2091–2107.

Ntaflos T., Keil K. and Newsom H. E. (1988) Khor Temiki: an enstatite achondrite with evidence of mixing of metal and sulfides from separate sources. *19th Lunar and Planet. Sci. Conf.*, 870–871.

Okada A. and Keil K. (1982) Caswellsilverite, $NaCrS_2$: a new mineral in the Norton County enstatite achondrite. *Am. Min.* **67**, 132–136.

Okada A., Keil K., Leonard B. F. and Hutcheon I. D. (1985) Schoellhornite, $Na_{0.3}(H_2O)_1[CrS_2]$, a new mineral in the Norton County enstatite achondrite. *Am. Mineral.* **70**, 638–643.

Okada A., Keil K., Taylor G. J. and Newsom H. (1988) Igneous history of the aubrite parent asteroid: evidence from the Norton County enstatite achondrite. *Meteoritics* **23**, 59–74.

Raghavan V. (1988) C–Fe–S (carbon–iron–sulphur) system. *J. Alloy Phase Diagrams* **4**(2), 133–142.

Reid A. M. and Cohen A. J. (1967) Some characteristics of enstatite from enstatite achondrites. *Geochim. Cosmochim. Acta* **31**, 661–672.

Richter G., Wolf R. and Anders E. (1979) Aubrites: are they direct nebular condensates? *10th Lunar and Planet. Sci. Conf.*, 1028–1030.

Righter K. (2003) Metal–silicate partitioning of siderophile elements and core formation in the early Earth. *Annu. Rev. Earth Planet. Sci.* **31**, 135–174.

Righter K. and Drake M. J. (2000) Metal/silicate equilibrium in the early Earth – new constraints from the volatile moderately siderophile elements Ga, Cu, P, and Sn. *Geochim. Cosmochim. Acta* **64**(20), 3581–3597.

Righter K., Humayun M. and Danielson L. R. (2008) Partitioning of palladium at high pressures and temperatures during core formation. *Nat. Geosci.* **1**, 321–323, doi:10.1038/ngeo18.

Righter K., Pando K. M., Danielson L. and Lee C. T. (2010) Partitioning of Mo, P and other siderophile elements (Cu, Ga, Sn, Ni, Co, Cr, Mn, V, and W) between metal and silicate melt as a function of temperature and silicate melt composition. *Earth Planet. Sci. Lett.* **291**(1–4), 1–9.

Rubin A. E. (1983) Impact melt–rock clasts in the Hvittis enstatite chondrite breccis: implications for a genetic relationship between EL chondrites and aubrites. *J. Geophys. Res.* **88**(Suppl.), 293–300.

Rubin A. E. (2010) Impact melting in the Cumberland Falls and Mayo Belwa aubrites. *Meteorit. Planet. Sci.* **45**, 265–275.

Shaw D. M. (1970) Trace element fractionation during anatexis. *Geochim. Cosmochim. Acta* **34**(2), 237–243.

Shen J. J., Papanastassiou D. A. and Wasserburg G. J. (1996) Precise Re–Os determinations and systematics of iron meteorites. *Geochim. Cosmochim. Acta* **60**(15), 2887–2900.

van Acken D., Brandon A. D. and Humayun M. (2011) High-precision osmium isotopes in enstatite and Rumuruti chondrites. *Geochim. Cosmochim. Acta* **75**(14), 4020–4036.

van Niekerk D., Humayun M., and Keil K. (2009) In situ determination of siderophile trace elements in EL3 meteorites. *40th Lunar and Planet. Sci. Conf.* #2049 (abstr.).

Wasson J. T. (1990) Ungrouped iron meteorites in Antarctica: origin of anomalously high abundance. *Science* **249**, 900–902.

Wasson J. T. and Kallemeyn G. W. (1988) Compositions of chondrites. *Philos. Trans. R. Soc. London, Ser. A* **A325**, 535–544.

Wasson J. T. and Wai C. M. (1970) Composition of metal, schreibersite and perryite of enstatite achondrites and the origin of enstatite chondrites and achondrites. *Geochim. Cosmochim. Acta* **34**, 169–184.

Watters T. R. and Prinz M. (1979) Aubrites: their origin and relationship to enstatite chondrites. *10th Lunar and Planet. Sci. Conf.*, 1073–1093.

Watters T. R. and Prinz M. (1980) Mt. Egerton and the aubrite parent body. *11th Lunar and Planet. Sci. Conf.*, 1225–1226.

Weisberg M. K., Prinz M., Clayton R. N., Mayeda T. K., Grady M. M., Franchi I., Pillinger C. T. and Kallemeyn G. W. (1996) The K (Kakangari) chondrite grouplet. *Geochim. Cosmochim. Acta* **60**(21), 4253–4263.

Wheelock M. M., Keil K., Floss C., Taylor G. J. and Crozaz G. (1994) REE geochemistry of oldhamite-dominated clasts from the Norton County aubrite: igneous origin of oldhamite. *Geochim. Cosmochim. Acta* **58**, 449–458.

Willis J. and Goldstein J. I. (1982) The effects of C, P, and S on trace-element partitioning during solidification in Fe–Ni alloys. *J. Geophys. Res.* **87**, A435–A445.

Wolf R., Ebihara M., Richter G. R. and Anders E. (1983) Aubrites and diogenites: trace element clues to their origin. *Geochim. Cosmochim. Acta* **47**, 2257–2270.

Zellner B., Leake M., Morrison D. and Williams J. G. (1977) E-asteroids and origin of enstatite achondrites. *Geochim. Cosmochim. Acta* **41**(12), 1759–1767.

Associate editor: Richard J. Walker